

1 **Radiation responses of 2D and 3D glioblastoma cells: a novel, 3D-specific**  
2 **radioprotective role of VEGF/Akt signaling through functional activation of**  
3 **NHEJ**

4 1. Natividad Gomez-Roman

5 2. Ming Y Chong

6 3. Sandeep K Chahal

7 4. Seamus P Caragher

8 5. Mark R Jackson

9 6. Katrina H Stevenson

10 7. Sidhartha A Dongre

11 8. Anthony J Chalmers

12 **Author affiliations:** <sup>1–8</sup> Wolfson Wohl Translational Cancer Research Centre,  
13 Institute of Cancer Sciences, University of Glasgow

14 **Running Title:** VEGF/Akt radioprotects 3D glioblastoma cells through NHEJ

15 **Keywords:** Glioblastoma, three-dimensional, VEGF, ionising radiation, DNA-PKcs

16 **Corresponding author:** Natividad Gomez-Roman, Wolfson Wohl Translational  
17 Cancer Research Centre, Institute of Cancer Sciences, University of Glasgow,  
18 Gartcube Estate, Glasgow G61 1BD. Email: [n.gomez-roman@beatson.gla.ac.uk](mailto:n.gomez-roman@beatson.gla.ac.uk);  
19 [Tel. 00 44 141 3303984](tel:00441413303984)

20 **Potential conflicts of interest:** The authors declare no potential conflicts of interest.

21

22 **Abstract**

23 Glioblastoma is resistant to conventional treatments and has dismal prognosis.  
24 Despite promising in vitro data, molecular targeted agents have failed to improve  
25 outcomes in patients, indicating that conventional two-dimensional (2D) in vitro  
26 models of GBM do not recapitulate the clinical scenario. Responses of primary  
27 glioblastoma stem-like cells (GSC) to radiation in combination with EGFR, VEGF and  
28 Akt inhibition were investigated in conventional 2D cultures and a 3-dimensional (3D)  
29 *in vitro* model of GBM that recapitulates key GBM clinical features. VEGF  
30 deprivation had no effect on radiation responses of 2D GSC but enhanced  
31 radiosensitivity of GSC cultures in 3D. The opposite effects were observed for EGFR  
32 inhibition. Detailed analysis of VEGF and EGF signalling demonstrated a  
33 radioprotective role of Akt that correlates with VEGF in 3D and with EGFR in 2D. In  
34 all cases, positive correlations were observed between increased radiosensitivity,  
35 markers of unrepaired DNA damage and persistent phospho-DNA-PK nuclear foci.  
36 Conversely, increased numbers of Rad51 foci were observed in radioresistant  
37 populations, indicating a novel role for VEGF/Akt signalling in influencing  
38 radiosensitivity by regulating the balance between non-homologous end-joining and  
39 homologous recombination mediated DNA repair. Differential activation of tyrosine  
40 kinase receptors in 2D and 3D models of GBM explains the well documented  
41 discrepancy between pre-clinical and clinical effects of EGFR inhibitors. Data  
42 obtained from our 3D model identify novel determinants and mechanisms of DNA  
43 repair and radiosensitivity in GBM, and confirm Akt as a promising therapeutic target  
44 in this cancer of unmet need.

45

46

47

## 48 **Introduction**

49 Glioblastoma (GBM) is the most common and aggressive malignant primary brain  
50 tumour <sup>1</sup>. Tumours exhibit inherent resistance to radiation and chemotherapy with 5  
51 year survival rates of ~4% <sup>2,3</sup>. Radiation resistance of GBM has been attributed to a  
52 subpopulation of cancer cells termed 'GBM stem-like cells' (GSC) which express  
53 stem cell markers, can differentiate into different lineages and have potent  
54 tumorigenic capacity <sup>4-10</sup>. To improve clinical outcomes, the molecular mechanisms  
55 underlying radio- and chemoresistance of GSC need to be elucidated. However,  
56 novel targeted agents that have shown pre-clinical activity in conventional GBM cell  
57 culture systems have consistently failed to achieve clinical efficacy.

58 One explanation for the discrepancy between preclinical and clinical data is the  
59 widespread use of preclinical models that fail to recapitulate the *in vivo* scenario.  
60 Lack of clinical efficacy of new agents might be explained by misleading preclinical  
61 data generated in established cancer cell lines cultured in simplified two-dimensional  
62 (2D) *in vitro* systems, in which cells undergo profound phenotypical changes and  
63 exhibit markedly different responses to cytotoxic treatments <sup>11-14</sup>. In the context of  
64 radiation therapy, 3D culture of lung and head & neck cancer cells embedded in  
65 laminin-rich extracellular matrix (lrECM) has been shown to promote radiation  
66 resistance compared to 2D culture <sup>15,16</sup>. Likewise, colorectal cancer cell lines  
67 cultured under similar 3D conditions exhibited changes in cellular morphology,  
68 phenotype and gene expression and were resistant to epidermal growth factor  
69 receptor (EGFR) inhibition compared to cells cultured in 2D conditions <sup>17</sup>. We have  
70 recently demonstrated lack of response to the EGFR tyrosine kinase inhibitor  
71 erlotinib either alone or in combination with radiation in a novel 3D model of GBM  
72 consisting of patient-derived GSC grown on 3D-Alvetex® scaffolds (3D), whereas

73 radiosensitisation was clearly observed in 2D GSC <sup>14</sup>. These findings recapitulate  
74 those of clinical trials in GBM in which treatments targeting EGFR either through the  
75 tyrosine kinase inhibitors erlotinib or gefitinib, or the anti-EGFR antibody cetuximab  
76 showed very low response rates and in some cases yielded inferior outcomes and/or  
77 worse toxicity than standard of care <sup>18-30</sup>, despite clear evidence of preclinical activity  
78 against established cell lines grown as 2D cultures. Taken together, these  
79 observations provide some insight into why results derived in conventional 2D cell  
80 culture systems are so often poorly predictive of clinical efficacy.

81 Anti-vascular endothelial growth factor (VEGF) therapy has also been evaluated in  
82 GBM, yielding marginally better clinical outcomes. Hypoxia is a cardinal feature of  
83 GBM, and is associated with high levels of vascular endothelial growth factor (VEGF)  
84 <sup>31,32</sup>. Increased VEGF expression correlates with poor prognosis and treatment  
85 resistance in GBM <sup>33,34</sup> and addition of anti-VEGF therapy (e.g. bevacizumab) to  
86 standard radio-chemotherapy increases progression-free survival but not overall  
87 survival <sup>35,36</sup>. While anti-VEGF therapy was developed primarily to target the tumour  
88 vasculature, GBM cells also express VEGF receptor 2 (VEGFR2) and are thus  
89 potential targets <sup>14,37</sup>, unlike normal brain in which VEGFR2 expression is  
90 undetectable. Previous studies have reported protective effects of VEGF on GBM  
91 cells treated with paclitaxel or radiation <sup>38</sup> that were mediated via VEGFR2. VEGFR2  
92 inhibition has also been shown to reduce GSC viability and survival *in vivo* <sup>37</sup>. We  
93 have recently added to this literature by showing that the anti-VEGF monoclonal  
94 antibody bevacizumab increases radiosensitivity in a customised 3D GSC system  
95 but has no effect in conventional 2D cultures <sup>14</sup>.

96 To interrogate these novel observations further, and elucidate the underlying  
97 mechanisms, we used our customised, validated 3D GBM model to investigate

98 whether the radiosensitising effects of VEGF inhibition are mediated via the DNA  
99 damage response (DDR). In this model, downregulation of VEGF signalling  
100 consistently induced a radiosensitive phenotype that was associated with aberrant  
101 NHEJ, inhibition of HR and accumulation of unrepaired DNA damage. We went on to  
102 show that the radiosensitising effects of VEGF depletion in 3D and EGFR inhibition  
103 in 2D cultures are mediated by the downstream signalling protein Akt. In addition,  
104 our data indicate that radiation induced changes in the sub-cellular localisation of  
105 EGFR are regulated by VEGF signalling.

## 106 **Materials and Methods**

### 107 **Cell Culture and Radiation Treatment**

108 E2, R10 and G7 GBM cell lines were obtained from Colin Watts laboratory, derived  
109 from anonymised patient resection specimens as previously described<sup>39</sup>. Cell lines  
110 were routinely cultured on Matrigel™-coated plates (0.2347mg/ml in Adv/DMEM) in  
111 cancer stem cell optimised serum-free medium comprising Advanced/DMEM/F12  
112 medium (GIBCO) Supplemented with 1% B27 (Invitrogen), 0.5% N2 (Invitrogen),  
113 4µg/ml heparin, 10ng/ml fibroblast growth factor 2 (bFGF, Sigma), 20ng/ml epidermal  
114 growth factor (EGF, Sigma) and 1% L-glutamine and used for experiments between  
115 passage 3 and 8. For Alvetex® 3D cultures (3D-A), Alvetex® scaffolds were coated  
116 with diluted Matrigel™ as for 2D conditions. Cells were irradiated using an RS225  
117 XStrahl machine, at 195 kV, 15 mA with a 0.5 copper filter, at a dose of 2.47 Gy/min.  
118 Cells were routinely tested every three months for mycoplasma always tested  
119 negative for mycoplasma contamination. Authentication of cells with Illumina  
120 Infinium Methylation Analysis in 2017.

### 121 **Mouse experiments**

122 Female CD1 nude mice were anaesthetised using isofluorane and a 1cm incision  
123 was made through the skin along the length of the skull. A hole was drilled through  
124 the skull 3 mm posterior to the bregma, and 2 mm lateral to the midline. Inoculation  
125 of tumour cells was performed using a digital stereotaxic frame (Harvard Apparatus).  
126 A programmable injector pump (Harvard Apparatus) was used to inject  $1 \times 10^5$  GSC in  
127  $5 \mu\text{l}$  PBS 3mm deep into the brain at a rate of  $2 \mu\text{l}/\text{min}$ .

128 Partial brain irradiation encompassing xenograft tumours was performed using the  
129 XStrahl small animal radiation research platform (SARRP). Mice were irradiated with  
130 220 kV (peak) X-ray beams at a dose of 4.8 Gy/min using a 5x5 mm collimator with  
131 parallel opposed beams under the guidance of cone-beam CT.

132

### 133 **Ethical approval**

134 Animal experiments were in compliance with all regulatory guidelines, as described  
135 in the Animals Act 1986 Scientific Procedures on living animals regulated by the  
136 Home Office in the United Kingdom.

137

### 138 **Clonogenic assays**

139 Cells were seeded on Matrigel<sup>TM</sup>-coated plates / 3D-Alvetex scaffolds (0.2374mg/ml).  
140 Seeding densities were as follows; 0-2 Gy – 300 cells / well (c/w); 3 Gy, 500 c/w; 4  
141 Gy, 800 c/w; 5-9 Gy, 1000 c/w. 18 hrs after seeding, cells were either sham  
142 irradiated or irradiated at indicated doses and incubated for 2.5 (2D) or 3 weeks (3D)  
143 prior to fixation with methanol and crystal violet staining for 2D conditions, or  
144 thiazolyl blue tetrazolium bromide (MTT) staining followed by 2% paraformaldehyde  
145 (PFA)/PBS for 3D conditions. Visible colonies were manually counted. Dose  
146 modifying factor (DMF) at 0.37% and 0.1% survival were calculated for each

147 treatment combination as well as sensitizing enhancement ratio (SER) to whole  
148 curve as in <sup>40</sup>.

149 For knockdown experiments, cells were transfected with respective siRNAs ( Table  
150 S1A) using Lipofectamine RNAiMax reagent according to manufacturer's instructions.  
151 After 48 h incubation, cells were detached with Accutase, counted and seeded in 3D-  
152 Alvetex Scaffolds at corresponding densities. 18 h after seeding, cells were  
153 irradiated at different doses (0-5 Gy) and incubated for 3 weeks. Clonogenic survival  
154 graphs represent mean plus SD of 3 independent experiments. Curves are fitted to a  
155 linear quadratic model and are normalised to respective 0 Gy control.

156 For 96-well clonogenics, cells were seeded (G7 -100 c/w, G1 – 200 c/w), incubated  
157 for 16 h, treated with respective compounds, incubated for 2 h, irradiated at 0 or 3  
158 Gy, and incubated for 13 days prior to colony staining and fixing.

159 Data was analysed using the median effect dose  
160 ([https://pdfs.semanticscholar.org/6e6f/5f9d670c203ade39e49dec5920fc759d5b67.p](https://pdfs.semanticscholar.org/6e6f/5f9d670c203ade39e49dec5920fc759d5b67.pdf)  
161 [df](https://pdfs.semanticscholar.org/6e6f/5f9d670c203ade39e49dec5920fc759d5b67.pdf)) and Bonferroni's statistical test.

## 162 **Immunofluorescence**

163 Cells ( $5 \times 10^4$  c/w) were seeded on Matrigel-coated coverslips or Matrigel-coated  
164 Alvetex® Scaffolds were exposed to erlotinib (1  $\mu$ M), MK-2206 with a chemical name  
165 of 8-[4-(1-aminocyclobutyl)phenyl]-9-phenyl-1,2,4-triazolo[3,4-*f*][1,6]naphthyridin-  
166 3(2*H*)-one hydrochloride [1:1] <sup>41</sup>(1  $\mu$ M) or vehicle and treated with 5 Gy or sham  
167 irradiated. Cultures were fixed in 2% PFA/PBS at the indicated time points,  
168 permeabilised with 1% Triton/PBS, blocked with 2% BSA/TBS/0.5% Tween-20 and  
169 incubated with the respective primary antibodies, followed by appropriate secondary

170 Alexa Fluor 568 or 488 secondary antibodies (Invitrogen, 1:400). Nuclei were  
171 counterstained with DAPI in mounting medium (VectaShield). For  $\gamma$ H2AX, pDNA-PK  
172 and Rad51 foci quantification Z-stacks were obtained at 63 $\times$  magnification on a  
173 Zeiss 780 confocal microscope. The number of nuclei analysed for each data point  
174 ranged from 30 to 50 nuclei. Foci per nucleus were counted manually.

175 For mitotic catastrophe, micronuclei and mitotic analysis, 3D cells were grown in  
176 Alvetex scaffolds for 4 days and then mock-irradiated or irradiated (5 Gy). Cells  
177 were fixed with 4% paraformaldehyde 24 h after radiation treatment. Scaffolds were  
178 immunostained for the mitotic marker phospho-S10 histone H3 (green) to visualise  
179 mitotic and mitotic catastrophe cells. DAPI was used to stain for DNA (blue). An  
180 average of 350 nuclei / condition / experiment were identified randomly and scored.  
181 Percentages of cells displaying micronuclei, mitosis or mitotic catastrophe per  
182 nucleus were calculated. Mean  $\pm$  SEM of 3 independent experiments. *P* values  
183 calculated by *t* test.

#### 184 **Protein extraction**

185 2D and 3D cells were exposed to the indicated treatments. For 2D cultures, cells  
186 were incubated for 30 minutes in lysis buffer (1% SDS-Tris buffer in the presence of  
187 phosphatase and protease inhibitors), scraped from plastic and clarified using  
188 Qiagen columns. For 3D cultures, scaffolds were incubated in lysis buffer for 25 min  
189 on ice, transferred to a rotating platform at 100 rpm and incubated for 5 minutes.  
190 Recovered lysate was clarified using Qiagen columns as for 2D lysates. Lysates  
191 were prepared using LDS sample buffer (Life Technologies) in the presence of 1  $\mu$ M  
192 DTT, blotted onto nitrocellulose membrane and probed with specific antibodies  
193 (Table S1B).

194

## 195 **Results**

### 196 **Differential radiosensitisation by erlotinib and VEGF in 2D and 3D cultures**

197 Elevated VEGF levels are a prominent feature of GBM in general and the GBM stem  
198 cell niche in particular, with concentrations reaching above 6000 pg/ml in these  
199 tumours <sup>31</sup>. VEGF has been shown to promote self-renewal and survival of GBM  
200 cancer stem cells <sup>37</sup> but its impact on their radiation responses is not well  
201 characterized. To evaluate whether clinically relevant concentrations of VEGF  
202 modulate cellular responses to radiation *in vitro*, effects on clonogenic survival of  
203 three different patient-derived GBM cell lines (G7, E2 and R10) were measured  
204 under 2D GSC culture conditions and in our novel 3D model <sup>14</sup>. Initially, we  
205 performed ELISA assays to measure secretion of VEGF. While all cell lines secreted  
206 VEGF in both hypoxic and normoxic conditions, concentrations were significantly  
207 lower than have been observed in GBM *in vivo* (Supplementary Fig. S1A). To  
208 recapitulate clinically observed levels of VEGF, therefore, media were supplemented  
209 with human recombinant VEGF-A (3000 pg/ml). Whereas VEGF supplementation  
210 had no effect on clonogenic formation of 2D or 3D GSC in the absence of radiation  
211 treatment (Fig. 1A), and did not affect radiosensitivity of 2D cultures, VEGF  
212 deprivation was associated with a significant increase in radiation sensitivity of 3D  
213 cultures in all three cell lines (Fig. 1B and Supplementary Table S2A). These data  
214 are consistent with our previous findings in which bevacizumab caused  
215 radiosensitisation in 3D cultures only <sup>14</sup>.

216 EGFR overexpression and/or gene amplification are also common features of GBM.  
217 Inhibition of EGFR activity with the specific tyrosine kinase inhibitor erlotinib

218 decreased phosphorylation of its active site (Y1173) at baseline and in irradiated  
219 conditions in both 2D and 3D GSC (Fig. 1C). However, radiosensitisation by erlotinib  
220 (1  $\mu$ M) was only observed in 2D cells (Fig. 1D and Supplementary Table S2B), as  
221 previously demonstrated<sup>14</sup>. A likely role for DNA repair in determining selective  
222 radiosensitisation of 2D cells by erlotinib was indicated by the observed delay in DSB  
223 resolution in 2D cells, as measured by sustained elevation of  $\gamma$ H2AX expression in  
224 protein extracts (Fig. 1C, compare lane 8 to lane 3). In marked contrast, erlotinib-  
225 treated 3D GSC appeared to exhibit faster resolution of  $\gamma$ H2AX expression than  
226 controls (Fig. 1C, compare lane 11 to lane 16).

227 To rule out the possibility that lack of radiosensitisation by erlotinib in 3D conditions  
228 was due to decreased drug delivery via compound adsorption to the scaffold, we  
229 assessed the radiosensitising activity of erlotinib alongside two known  
230 radiosensitisers, the PARP inhibitor olaparib and the ATM inhibitor KU-55933<sup>42</sup>,  
231 across a range of concentrations. Reduced clonogenic efficiency was detected at 3  
232 Gy as expected (Supplementary Fig. S1B). Erlotinib failed to induce  
233 radiosensitisation of 3D cultures even at the highest concentration tested (10  $\mu$ M,  
234 Supplementary Fig. S1C), whereas radiosensitisation could be detected with  
235 olaparib and KU55933 at nanomolar and micromolar concentrations, respectively  
236 (Supplementary Fig. S1D and S1E). These results validate our conclusion that  
237 erlotinib has no radiosensitising effect on 3D cells, and render any effect of the  
238 scaffold on drug activity very unlikely.

## 239 **Differential regulation of the downstream signalling molecule Akt in 2D and 3D** 240 **GSC**

241 In order to characterise the mechanisms by which VEGF and EGFR regulate GSC  
242 radiosensitivity we interrogated their key downstream signalling pathway Akt. G7  
243 and E2 cells grown in 2D or 3D conditions were starved of growth factors for 48  
244 hours then induced either with EGF or with VEGF. While EGF treatment induced  
245 robust activation of EGFR and phosphorylation of Akt at the early time points in cells  
246 grown in 2D conditions, addition of VEGF showed no increment in Akt activation  
247 beyond baseline levels (Fig. 2A, left side blots). In contrast, 3D cells showed robust  
248 Akt activation upon VEGF stimulation in both G7 and E2 cells (Fig. 2A, right hand  
249 blots). EGF stimulation had a modest positive impact on Akt phosphorylation in G7  
250 3D cells at the early time points (Fig. 2A, left panels), remaining at baseline levels in  
251 E2 3D cells. Expression of the three Akt isoforms at both mRNA and protein levels  
252 was observed in G7 and E2 cell lines (Supplementary Fig. S2A and S2B).  
253 Enrichment analysis<sup>43</sup> of RNASeq data derived from G7 and E2 3D cells before and  
254 after radiation treatment revealed upregulation of genes involved in the Akt pathway  
255 (Supplementary Fig. S2C), supporting a likely role for Akt signalling in mediating  
256 radiation responses of 3D GSC.

257 The divergent effects of EGFR inhibition on radiosensitivity of 2D and 3D GSC  
258 cultures prompted us to investigate how the radiation-erlotinib combination affected  
259 Akt signalling in these two systems. Erlotinib titration (0.5  $\mu$ M to 5  $\mu$ M) showed  
260 inhibition of EGFR activity in both 2D and 3D cultures, as demonstrated by  
261 decreased phosphorylation of its active site (Y1173) both at baseline and after  
262 radiation (Fig. 2B). However, this effect only translated into attenuation of Akt  
263 activation in 2D cells, having no effect on Akt activity in the 3D model in the G7 cell  
264 line and a reduced effect in E2 cells (Fig. 2B). This is in keeping with our previous  
265 observation that EGF plays only a minor role in Akt activation in the 3D system (Fig.

266 2A). Time course analysis revealed inhibition of radiation induced Akt activity by  
267 erlotinib in 2D conditions at early time points (30 min to 3 hrs) (Fig. 2C, left panels),  
268 but no effect in 3D conditions (Fig. 2C, right panels). Baseline levels of total Akt  
269 were similar in 2D and 3D cells (Fig. 2C). Taken together, our results suggest that  
270 Akt activity is differentially regulated in 2D and 3D conditions: by EGF signalling in  
271 2D conditions; and by VEGF signalling in 3D cells.

### 272 **Akt regulates radiation resistance in 2D and 3D GSC**

273 Having identified a pivotal role for Akt in downstream signalling from VEGF and  
274 EGFR, we next investigated its contribution to radiation resistance of 2D and 3D  
275 GSC using the specific Akt1/2 inhibitor MK-2206. Treatment of G7 and E2 GSC with  
276 MK-2206 (1  $\mu$ M) consistently inhibited Akt activity in all models, as demonstrated by  
277 reduced phosphorylation (Fig. 2D). This effect was accompanied by  
278 radiosensitisation in all models (Fig. 3A and 3B, Supplementary Table S2C). In the  
279 case of G7 cells, radiosensitisation was not further increased by erlotinib in 2D  
280 conditions (Fig. 3A, left graphs) or by VEGF deprivation in 3D conditions (Fig. 3B, left  
281 graph). MK-2206 had more pronounced radiosensitising effects on E2 2D cells than  
282 erlotinib alone or indeed erlotinib in combination with MK-2206 (Fig. 3A, right graph  
283 and Supplementary Table S2C), suggesting that other unidentified upstream  
284 signalling factors may be regulating Akt activity in this cell line. In 3D E2 cells, MK-  
285 2206 alone and VEGF-deprivation exhibited similar radiosensitising effects whilst the  
286 combination of MK-2206 and VEGF-deprivation induced further radiosensitisation  
287 (Fig. 3B, right graph and Supplementary Table S2C). These results indicate additive  
288 effects of VEGF and Akt inhibition in this cell line. Subsequent experiments  
289 confirmed a dose response for the radiosensitizing effect of MK-2206 (Fig. 3C).

290 To validate that the radiosensitizing effects of MK-2206 were 'on target', the effects  
291 of Akt knockdown were evaluated using siRNA targeting of the three Akt isoforms.  
292 Downregulation of Akt1 and Akt3 expression at the protein level was detected in E2  
293 cells (Fig. 3D) and was associated with radiosensitisation of E2 3D GSCs (Fig. 3E  
294 and Supplementary Table S2D) validating the effects of MK-2206 treatment.  
295 Radiosensitising effects were also observed with the Akt inhibitor perifosine  
296 (Supplementary Fig. S2D) further confirming the radiosensitising effects of this class  
297 of compounds. Overall, these results indicate that radiation sensitivity in GSC is  
298 modulated by Akt activity irrespective of the growth conditions.

299 **VEGF deprivation and Akt inhibition are associated with reduced DSB repair**  
300 **and increased mitotic catastrophe in irradiated 3D GSC**

301 Radiation kills cells by damaging DNA and the integrity of the DNA damage  
302 response (DDR) is a key determinant of radiosensitivity. More specifically, DNA  
303 double strand breaks (DSB) are the most important cytotoxic lesions induced by  
304 radiation and are repaired either by the rapid but error-prone non-homologous end-  
305 joining (NHEJ) pathway or by homologous recombination (HR) which is accurate but  
306 slower and requires the presence of a homologous sister chromatid <sup>44,45</sup>. To  
307 investigate the mechanisms underlying the radiosensitising effects of VEGF  
308 deprivation and Akt inhibition, quantitative analysis of induction and resolution of  
309 radiation induced DSB was performed, using nuclear  $\gamma$ H2AX foci as markers of DSB.  
310 Delayed resolution of DSB was observed in the VEGF-deprived radiosensitive  
311 population compared to the radioresistant VEGF-supplemented 3D populations as  
312 shown by increased numbers of unresolved  $\gamma$ H2AX foci 24 hours after irradiation (Fig.  
313 4A and B). The possibility that this increase in  $\gamma$ H2AX foci was due to a larger  
314 proportion of VEGF-deprived cells being in the G2 phase of the cell cycle was

315 excluded by the fact that similar percentages of cells staining positive for the G2  
316 phase marker CENPF were detected in both conditions (Supplementary Fig. S3A  
317 and S3B, VEGF-enriched 24.44%  $\pm$ 7.62, VEGF-deprived 22.985%  $\pm$ 1.138). No  
318 significant differences in  $\gamma$ H2AX foci were observed in VEGF-deprived or  
319 supplemented cells in the absence of radiation (Fig. 4C). A delay in DSB resolution  
320 was also observed in 3D (Fig. 4D) and 2D cells (Fig. 4E) treated with MK-2206 (1  
321  $\mu$ M). More detailed analysis revealed MK-2206 to be associated with increased  
322 numbers of  $\gamma$ H2AX foci 30 minutes after radiation, suggesting either increased  
323 induction of DSB or impairment of early (or 'fast') DSB repair, and at the 24 hour time  
324 point (Fig. 4E; representative images in Supplementary Fig. S3C). Unirradiated  
325 GSCs treated with MK-2206 exhibited a small but statistically significant increase in  
326 median number of foci compared to vehicle at the 24 hour time point, indicating a  
327 possible role for Akt in repair of DSB arising from endogenous sources (Fig. 4F).

328 Levels of unresolved DSB at 24 hours correlate with radiation sensitivity both *in vitro*  
329 and *in vivo* <sup>44</sup> and have potential to cause cell death by a number of mechanisms  
330 including mitotic catastrophe <sup>46,47</sup>. To understand the cell death mechanisms by  
331 which inhibition of VEGF or Akt signalling enhances radiosensitivity, quantification of  
332 mitotic cells and those undergoing mitotic catastrophe was performed using the  
333 specific mitotic marker histone H3 phosphorylated at serine 10 (pS10-H3). Cells  
334 undergoing mitotic catastrophe were readily detected as fragmented, pS10-H3  
335 positive nuclei (Fig. 4G, red arrows). Whereas numerous cells undergoing mitotic  
336 catastrophe were identified in VEGF-deprived 3D cultures 24 hours after irradiation,  
337 very few were observed in VEGF-enriched 3D conditions (Fig. 4G and H). An  
338 increase in the number of cells exhibiting micronuclei was also observed in the  
339 VEGF-deprived populations (Fig. 4H), consistent with the hypothesis that cells

340 completing mitosis in the presence of unrepaired DNA DSBs generate severe  
341 structural chromosomal defects and will eventually succumb. Similar increases in  
342 micronuclei were observed in irradiated cells treated with MK-2206 (Supplementary  
343 Fig. S3D). Together these results demonstrate that VEGF-deprived 3D cells and Akt  
344 inhibited cells are less efficient at repairing radiation induced DNA damage and  
345 hence accumulate unresolved DNA DSB that lead eventually to cell death by  
346 mechanisms including mitotic catastrophe.

347 **Aberrant NHEJ characterised by persistent DNA-PKcs binding at DSB is**  
348 **associated with the radiosensitising effects of VEGF deprivation or MK-2206**  
349 **treatment**

350 Cell survival after radiation is determined by both induction of DNA damage and the  
351 repair processes that follow. Efficiency and integrity of DSB repair depend on  
352 appropriate engagement of either NHEJ or HR, and it has been reported that cancer  
353 cells can be susceptible to aberrant DSB repair as a consequence of over-  
354 expression or inappropriate activation of NHEJ proteins <sup>48,49</sup>. Approximately 80% of  
355 X-ray-induced DSBs are repaired within 2-3 hours by the NHEJ pathway, of which  
356 DNA-PKcs is a major catalytic component <sup>50</sup>. Of direct relevance to our experiments,  
357 Akt has been shown to activate DNA-PKcs activity in response to radiation <sup>51,52</sup>. To  
358 investigate whether delayed resolution of DSBs in the radiosensitised populations  
359 was due to diminished NHEJ repair, we quantified the number of phosphorylated  
360 DNA-PKcs foci per nucleus in G7 and E2 cells. Unexpectedly, the number of pDNA-  
361 PKcs foci 0.5 hours after radiation (5 Gy) was found to be significantly increased in  
362 VEGF-deprived, radiosensitive 3D populations compared to the more radioresistant  
363 VEGF-enriched 3D cells (Fig. 5A and B). In contrast, VEGF treatment did not affect  
364 the number of pDNA-PKcs foci in 2D cultures (Supplementary Fig. S3E).

365 Quantitative analysis of pDNA-PKcs kinetics over a 24 hour period after radiation  
366 treatment showed increased numbers of foci throughout the time course in the  
367 radiosensitive VEGF-deprived 3D GSC populations compared to 3D cells grown in  
368 the presence of VEGF (Fig. 5A and B). We hypothesized that the presence of large  
369 numbers of unresolved pDNA-PKcs foci in VEGF-deprived 3D cells at the 24 hour  
370 time point was indicative of ineffective attempts at DSB repair, an interpretation that  
371 is supported by the  $\gamma$ H2AX data shown in Fig. 3 and the additional observation that  
372 these unresolved pDNA-PKcs foci were larger than those observed at earlier time  
373 points (Fig 5A, compare 0.5 hrs (-) VEGF image with 24 hrs (-) VEGF image).  
374 Consistent with our previous results, we observed a similar increase in the number of  
375 pDNA-PKcs foci (red) at the 24 hrs time point in MK-2206 treated 3D cells compared  
376 to controls (Fig. 5C). These foci co-localised with  $\gamma$ H2AX foci (green), indicating that  
377 pDNA-PKcs molecules were accumulating at DSB (Fig. 5C). In order to validate that  
378 these DNA-PK foci mediated radiosensitising effects were occurring downstream of  
379 VEGF and Akt, clonogenic assays were performed in cells depleted of DNA-PKcs by  
380 siRNA targeting. Following siRNA transfection, E2 cells exhibited a significant  
381 reduction in DNA-PKcs protein expression and were more radiosensitive than cells  
382 transfected with scrambled siRNA (Fig. 5D). Importantly, whereas MK-2206  
383 mediated radiosensitisation persisted in cells expressing scrambled siRNA, no  
384 additional radiosensitisation was observed in cells depleted of DNA-PKcs (Fig. 5D  
385 and Supplementary Table S2E). These data provide compelling evidence for a novel  
386 role for VEGF/Akt signalling in influencing radiosensitivity by interfering with NHEJ  
387 through persistent binding of DNA-PKcs to DSB. We postulate that this role has not  
388 been identified previously because mechanistic studies have generally been

389 conducted in 2D *in vitro* cultures in which EGFR signalling is upregulated at the  
390 expense of VEGF signalling.

### 391 **Homologous recombination repair is regulated by VEGF in 3D cultures**

392 It is well established that the NHEJ and HR pathways 'compete' for access to and  
393 repair of DSB under certain circumstances, and inhibition of NHEJ has been shown  
394 to enhance DSB repair under certain conditions by promoting HR<sup>53</sup>. To test the  
395 hypothesis that persistent binding of pDNA-PKcs to DSB inhibits HR repair function,  
396 3D cells in the presence or absence of VEGF were fixed 3 hours after radiation and  
397 stained for the key HR protein Rad51. While considerable numbers of Rad51 foci per  
398 nucleus were detected in the radioresistant VEGF enriched 3D cells, far fewer foci  
399 were visible in the radiosensitive VEGF-deprived 3D cultures at the same time point  
400 (Fig. 5E and F). These findings were supported by similar observations when cells  
401 were stained for an alternative HR protein BRCA2 (Supplementary Fig. S3F). This  
402 effect cannot be explained by a difference in cell cycle distribution as the proportion  
403 of CENPF positive G2 cells was not affected by VEGF addition (Supplementary Fig.  
404 S3A and S3B). Consistent with the tenet that HR is cell cycle phase specific,  
405 functioning only in S and G2 phases during which a sister chromatid DNA template is  
406 available for repair, the proportion of nuclei staining positive for Rad51 was not  
407 statistically significant to the proportion of CENPF positive cells under the same  
408 conditions (Supplementary Fig. S3G). These data indicate that, in this 3D model,  
409 VEGF-deprived cells initiate HR at a much lower rate than VEGF-enriched cells and  
410 are consistent with a scenario in which VEGF driven activation of Akt promotes rapid  
411 and efficient NHEJ, which also permits functional HR. In the absence of VEGF, lack  
412 of Akt signalling results in aberrant and prolonged binding of DNA-PKcs to DSB  
413 which both delays NHEJ mediated repair and inhibits HR.

414

415 **Activation of VEGFR2 and functional activation of both NHEJ and HR in an**  
416 **orthotopic mouse model of GBM**

417 To validate *in vivo* the observations made in the 3D model *in vitro*, we interrogated  
418 relevant DDR parameters before and after irradiation in tissue from patient-derived  
419 human GBM orthotopic mouse models. We have previously shown phosphorylation  
420 and activation of the VEGFR2 receptor in the majority of tumour cells in G7 and E2  
421 orthotopic tumours<sup>14</sup> and Supplementary Fig. S4A, confirming that VEGF/VEGFR2  
422 signalling is active *in vivo*. Based on our 3D *in vitro* data, we hypothesised that  
423 tumour cells in which VEGF signalling pathway is active would exhibit functional  
424 NHEJ and that pDNA-PKcs nuclear foci would be detectable at early time points  
425 after irradiation *in vivo* and would resolve rapidly. To assess this, CD1 nude mice  
426 were injected intracranially with E2 cells and monitored for five months to allow the  
427 infiltrative tumour growth pattern characteristic of this model. Following this period,  
428 mice underwent partial brain irradiation (10Gy) or mock treatment and were  
429 sacrificed at different time points (0, 0.5, 2 and 24 h). Immunofluorescence was  
430 performed to evaluate activation of NHEJ by detection of pDNA-PKcs nuclear foci.  
431 For this experiment, EGFR was selected as tumour cell marker as it was not  
432 expressed in normal mouse brain tissue (Supplementary Fig. S4A). A significant  
433 increase in pDNA-PKcs foci was detected 30 minutes after radiation treatment, the  
434 vast majority of which had resolved within 2 hours. No foci were detected at the 24  
435 hour time point (Fig. 6A). Consistent with these data, Rad51 nuclear foci were  
436 detected 4 hours after radiation treatment *in vivo* and had resolved by 24 hours  
437 (Supplementary Fig. S4B). These data recapitulate our *in vitro* observations, where  
438 3D GSC grown in the presence of VEGF activated Akt and exhibited efficient DSB

439 repair, with early NHEJ activation followed by HR activation and complete resolution  
440 of repair foci by 24 hours.

441 **MK-2206 extends survival in combination with radiation in the U87MGLuc**  
442 **orthotopic xenograft GBM model**

443 We then proceeded to evaluate the efficacy of combining Akt inhibition with radiation  
444 *in vivo*. CD1 nude mice were injected intracranially with U87MGLuc cells.  
445 Bioluminescence imaging was performed on day 6 confirming tumour engraftment  
446 (Supplementary Fig. S4C). At day 13, mice were randomised into 4 cohorts (Fig.  
447 6B), and treated with respective protocols over a two-week period. All treatment  
448 regimens were well tolerated, with no significant changes in body weight observed  
449 (Fig. 6C). Following this period, mice were monitored daily and sacrificed when  
450 symptomatic. While no increase in survival was conferred by the Akt inhibitor MK-  
451 2206 alone, the radiation schedule of 6 x 2 Gy (administered on alternate days) was  
452 associated with a modest but statistically significant increase in survival ( $P < 0.001$ ),  
453 and combined treatment with MK-2206 and radiation conferred additional survival  
454 benefit, with a 9-day prolongation in median survival over control or MK-2206 alone  
455 ( $P < 0.0001$ ) and a 5-day prolongation in median survival relative to the IR schedule  
456 ( $P = 0.006$ ; Fig. 6D and E, Supplementary Table S3).

457 **Erlotinib treatment of VEGF-deprived 3D GSC increases their radiation**  
458 **resistance**

459 While performing clonogenic assays with different treatment combinations, we  
460 observed that erlotinib had a marked radioprotective effect on VEGF-deprived 3D  
461 cultures in three different patient-derived cell lines (G7, E2, and R10), an effect of the  
462 same magnitude as that observed for VEGF treatment in this model (Fig 7A and

463 Supplementary Fig. S5A). No further radioprotection was detected in the presence  
464 of VEGF (Fig. 7A), indicating a correlation between VEGF signalling and EGFR  
465 inhibition that has not been documented previously. In contrast, radiosensitisation of  
466 2D cultures by erlotinib was not affected by VEGF (Supplementary Fig. S5B-D).  
467 Consistent with these results, the radioresistant erlotinib-treated 3D GSC and the 3D  
468 GSC supplemented with VEGF were more efficient at repairing DSBs after radiation  
469 treatment, exhibiting lower number of  $\gamma$ H2AX foci levels at 24 hrs than the  
470 radiosensitive 3D VEGF-deprived cells (Supplementary Fig. S5E). No statistically  
471 significant difference was observed in the number of pDNA-PKcs foci and Rad51 foci  
472 were observed in the erlotinib-treated VEGF-deprived 3D GSC (Fig. 7B and 7C) and  
473 in erlotinib-treated VEGF supplemented 3D GSC (Supplementary Fig. S5F and S5G)  
474 as in the VEGF-treated cells at early time points, which were completely resolved at  
475 24 hrs, in contrast to the VEGF-deprived cells without erlotinib which exhibited  
476 increased pDNA-PKcs foci at all timepoints and reduced Rad51 foci.

477 **EGFR/DNA-PKcs nuclear colocalisation correlates with aberrant NHEJ and HR**  
478 **in VEGF-deprived radiosensitive populations**

479 Having made the novel and unexpected observation that EGFR inhibition protected  
480 3D GSCs following ionising radiation, we investigated the mechanisms involved. In  
481 head and neck carcinomas, EGFR activates repair of radiation induced DSB through  
482 phosphorylation of DNA-PKcs [35, 36]. Colocalisation analysis of DNA-PKcs and  
483 EGFR was therefore performed in G7 and E2 3D cultures in the radioresistant  
484 populations (+VEGF or erlotinib) and the radiosensitive VEGF-deprived cells.  
485 Nuclear colocalisation of DNA-PKcs and EGFR was detected in the VEGF-deprived  
486 radiosensitive 3D populations at both early (0.5 hours) and late (24 hours) timepoints

487 after radiation treatment. In contrast, nuclear colocalisation of DNA-PKcs and EGFR  
488 could not be observed in the radioresistant G7 3D (Fig. 7D-F) or E2 3D  
489 (Supplementary Fig. S5H) populations either before or after irradiation. These  
490 findings suggest that, in a clinically relevant 3D model of GBM: (i) VEGF inhibits  
491 nuclear localisation of EGFR, (ii) EGFR activation is required for its translocation into  
492 the nucleus, and (iii) EGFR/DNA-PKcs complex binding to DSBs requires additional  
493 signalling that promotes its disassociation and functional DSB repair.

494

## 495 **Discussion**

496 Here we describe a novel role for VEGF/VEGFR2 signalling in the regulation of  
497 radiation sensitivity and the DDR using a customised, 3D cell culture system that  
498 resembles key histological features of GBM and replicates particular clinical  
499 responses to molecular targeted therapies such as EGFR inhibition and  
500 temozolomide treatment. Our results provide important insights into the mechanisms  
501 by which GSC survive radical radiotherapy. Anti-VEGF therapy (bevacizumab) was  
502 developed primarily to target angiogenesis; our 3D model identifies a direct effect of  
503 VEGF on tumour cell radiosensitivity that could be exploited to overcome radiation  
504 resistance. Credence for the clinical efficacy of targeting VEGF signalling in GBM is  
505 provided by recently reported results of a phase II study of the VEGFR, FGFR and  
506 PDGFR inhibitor regorafenib in patients with recurrent disease, which showed  
507 improved 12 month overall survival (38.9% vs 15.0%) and 6 month progression-free  
508 survival (16.9% vs 8.3%) compared with lomustine <sup>54</sup>. A number of potential  
509 resistance mechanisms may explain the failure of bevacizumab to extend survival in  
510 first line treatment (39), including failure to cross the blood brain barrier and

511 compensatory roles of other VEGFs (e.g. VEGF-B) or VEGF receptors. More  
512 specifically, GSC have been shown to exhibit a VEGF/VEGFR2 autocrine signalling  
513 loop associated with a cytosolic VEGFR2 subfraction <sup>37</sup>, which might contribute to  
514 resistance to VEGF targeting strategies. Our results indicate that tyrosine kinase  
515 receptor related mechanisms underlying radioresistance of GBM in general and GSC  
516 in particular are worthy of detailed investigation in the future. Further assessment in  
517 the 3D model of successful and failed molecular therapies in the clinic will provide  
518 meaningful validation of the 3D model for utilisation in preclinical studies of molecular  
519 targeted therapies that might predict translational success.

520 Radioresistance is intimately associated with the DDR, and efficiency and integrity of  
521 DSB repair depends on appropriate engagement of NHEJ and/or HR. An increasing  
522 body of evidence indicates that cancer cells might be susceptible to aberrant DSB  
523 repair as a consequence of over-expression or inappropriate activation of NHEJ  
524 proteins including the catalytic subunit DNA-PKcs <sup>51,52</sup>. While EGFR signalling has  
525 been shown to modulate DNA DSB repair in general and DNA-PKcs activity in  
526 particular <sup>51,52,55,56</sup>, to our knowledge there is no published evidence that VEGF  
527 signalling influences any aspect of DNA repair. Our previous observations with  
528 bevacizumab <sup>14</sup> and the demonstration by Bartek's group that direct inhibition of  
529 VEGFR2 reduces GSC viability under conditions of radiation-evoked stress, implied  
530 a potential role for VEGF in DNA repair. The data presented here demonstrate for  
531 the first time that VEGF can activate DNA repair via Akt and DNA-PKcs functionality,  
532 a phenomenon that is only observed in 3D conditions. Furthermore, our studies  
533 show for the first time that Akt responds to different cues in 2D and 3D cells. While  
534 EGFR regulated Akt activity in 2D cultures, VEGF signalling was required for its  
535 activation in the 3D model. Our results are consistent with previous reports that Akt

536 signalling to DNA-PK promotes functional NHEJ activity and radioprotection, but in  
537 previous studies conducted in 2D cultures, the link to VEGF signalling was not  
538 appreciated.

539 Several reports have demonstrated pre-clinical efficacy of the Akt MK-2206 inhibitor  
540 in combination with gefitinib) in mouse models of GBM<sup>57,58</sup>. Indeed, clinical trials  
541 investigating Akt inhibitors in the treatment of GBM are either underway or in  
542 development (e.g. <https://clinicaltrials.gov/ct2/show/NCT02430363>). Unfortunately a  
543 phase I study of MK-2206 in recurrent GBM was terminated prior to enrolment  
544 following a re-prioritisation process by the pharmaceutical company. Data from our  
545 3D model strongly support the hypothesis that inhibition of Akt will improve clinical  
546 outcomes for GBM and provide further justification for clinical trials in this area. They  
547 also indicate that the interplay between EGFR, VEGFR2, Akt and DNA-PKcs and  
548 possibly other tyrosine kinase receptors such as PDGF and FGFR is worthy of  
549 detailed investigation in the future.

550 Based on preclinical data, huge amounts of time and money have been devoted to  
551 clinical studies targeting EGFR in the treatment of GBM, none of which has been  
552 successful. In phase I/II clinical trials, addition of erlotinib to radiotherapy and  
553 temozolomide failed to improve outcomes<sup>21,22</sup> and in some cases yielded worse  
554 outcomes<sup>26</sup>. The identification in 2D breast and pancreatic cell culture systems of  
555 radiation-specific phosphorylation sites of EGFR (Y845 and T654)<sup>59</sup> that induce its  
556 translocation to the nucleus and stimulate activation of DNA-PKcs provided a  
557 detailed rationale and mechanism of action for combining EGFR inhibitors with  
558 radiation. Nuclear translocation of EGFR was observed after radiation treatment in  
559 VEGF-deprived, radiosensitive 3D cultures as opposed to VEGF supplemented,  
560 radioresistant cell populations suggests important cross-talk between EGFR and

561 VEGFR signalling in the 3D context and warrants further investigation. More  
562 generally, discrepancies between the EGFR signalling effects observed in our 3D  
563 cultures and those described in previous reports might explain the failure of  
564 simplified 2D preclinical models to predict the negative outcomes of clinical trials.

565 In summary, irradiation of GBM stem-like cells in a novel 3D cell culture system has  
566 radiosensitisation and revealed previously unreported radioprotective effects of  
567 VEGF that are mediate through the NHEJ and HR DNA repair pathways (Fig. 7G).  
568 As well as increasing our understanding of the clinical effects and limitations of  
569 radiation therapy in the management of patients with GBM, these data support the  
570 clinical evaluation of Akt inhibitors in GBM and reinforce the concept that potential  
571 treatments for GBM should be evaluated in more representative 3D models before  
572 proceeding to *in vivo* and clinical testing.

573

#### 574 **Acknowledgements**

575 Cell lines were kindly donated by Dr Colin Watts, University of Cambridge. This  
576 research was funded by a Chief Scientist Office (CSO, grant number ETM/405) to  
577 A.Chalmers. We also thank the National Centre for the Replacement, Refinement  
578 and Reduction of Animals in Research (NC3Rs) for funding this work (grant  
579 reference NC/P001335/1) to A.Chalmers and N. Gomez-Roman.

580

581

582

583 **References**

- 584 1 Brodbelt, A. *et al.* Glioblastoma in England: 2007-2011. *Eur J Cancer* **51**, 533-542,  
585 doi:10.1016/j.ejca.2014.12.014 (2015).
- 586 2 Stupp, R. *et al.* Effects of radiotherapy with concomitant and adjuvant temozolomide versus  
587 radiotherapy alone on survival in glioblastoma in a randomised phase III study: 5-year  
588 analysis of the EORTC-NCIC trial. *Lancet Oncology* **10**, 459-466, doi:Doi 10.1016/S1470-  
589 2045(09)70025-7 (2009).
- 590 3 Stupp, R. *et al.* Radiotherapy plus concomitant and adjuvant temozolomide for glioblastoma.  
591 *New England Journal of Medicine* **352**, 987-996, doi:Doi 10.1056/Nejmoa043330 (2005).
- 592 4 Zschenker, O., Streichert, T., Hehlgans, S. & Cordes, N. Genome-wide gene expression  
593 analysis in cancer cells reveals 3D growth to affect ECM and processes associated with cell  
594 adhesion but not DNA repair. *PLoS One* **7**, e34279, doi:10.1371/journal.pone.0034279 (2012).
- 595 5 Luca, A. C. *et al.* Impact of the 3D Microenvironment on Phenotype, Gene Expression, and  
596 EGFR Inhibition of Colorectal Cancer Cell Lines. *Plos One* **8** (2013).
- 597 6 Pontes Soares, C. *et al.* 2D and 3D-organized cardiac cells shows differences in cellular  
598 morphology, adhesion junctions, presence of myofibrils and protein expression. *PloS one* **7**,  
599 e38147 (2012).
- 600 7 Bao, S. *et al.* Glioma stem cells promote radioresistance by preferential activation of the  
601 DNA damage response. *Nature* **444**, 756-760, doi:10.1038/nature05236 (2006).
- 602 8 Eramo, A. *et al.* Chemotherapy resistance of glioblastoma stem cells. *Cell Death Differ* **13**,  
603 1238-1241, doi:10.1038/sj.cdd.4401872 (2006).
- 604 9 Lathia, J. D. *et al.* Direct in vivo evidence for tumor propagation by glioblastoma cancer stem  
605 cells. *PloS one* **6**, e24807 (2011).
- 606 10 Singh, S. K., Clarke, I. D., Hide, T. & Dirks, P. B. Cancer stem cells in nervous system tumors.  
607 *Oncogene* **23**, 7267-7273 (2004).
- 608 11 Bokhari, M., Carnachan, R. J., Cameron, N. R. & Przyborski, S. A. Culture of HepG2 liver cells  
609 on three dimensional polystyrene scaffolds enhances cell structure and function during  
610 toxicological challenge. *Journal of anatomy* **211**, 567-576 (2007).
- 611 12 Benton, G., George, J., Kleinman, H. K. & Arnaoutova, I. P. Advancing Science and Technology  
612 Via 3D Culture on Basement Membrane Matrix. *Journal of Cellular Physiology* **221**, 18-25,  
613 doi:Doi 10.1002/Jcp.21832 (2009).
- 614 13 Eke, I. & Cordes, N. Radiobiology goes 3D: how ECM and cell morphology impact on cell  
615 survival after irradiation. *Radiother Oncol* **99**, 271-278, doi:10.1016/j.radonc.2011.06.007  
616 (2011).
- 617 14 Gomez-Roman, N., Stevenson, K., Gilmour, L., Hamilton, G. & Chalmers, A. J. A novel 3D  
618 human glioblastoma cell culture system for modeling drug and radiation responses. *Neuro*  
619 *Oncol*, doi:10.1093/neuonc/now164 (2016).
- 620 15 Storch, K. *et al.* Three-dimensional cell growth confers radioresistance by chromatin density  
621 modification. *Cancer research* **70**, 3925-3934 (2010).
- 622 16 Hehlgans, S., Lange, I., Eke, I. & Cordes, N. 3D cell cultures of human head and neck  
623 squamous cell carcinoma cells are radiosensitized by the focal adhesion kinase inhibitor  
624 TAE226. *Radiother Oncol* **92**, 371-378, doi:10.1016/j.radonc.2009.08.001 (2009).
- 625 17 Poschau, M. *et al.* EGFR and beta1-integrin targeting differentially affect colorectal  
626 carcinoma cell radiosensitivity and invasion. *Radiother Oncol* **116**, 510-516,  
627 doi:10.1016/j.radonc.2015.06.005 (2015).
- 628 18 van den Bent, M. J. *et al.* Randomized phase II trial of erlotinib versus temozolomide or  
629 carmustine in recurrent glioblastoma: EORTC brain tumor group study 26034. *Journal of*  
630 *clinical oncology : official journal of the American Society of Clinical Oncology* **27**, 1268-1274  
631 (2009).
- 632 19 Rich, J. N. *et al.* Phase II trial of gefitinib in recurrent glioblastoma. *Journal of clinical*  
633 *oncology : official journal of the American Society of Clinical Oncology* **22**, 133-142 (2004).

- 634 20 Brewer, C. J. *et al.* Phase II trial of erlotinib with temozolomide and concurrent radiation  
635 therapy in patients with newly-diagnosed glioblastoma multiforme. *Journal of Clinical*  
636 *Oncology* **23**, 130s-130s (2005).
- 637 21 Peereboom, D. M. *et al.* Phase II trial of erlotinib with temozolomide and concurrent  
638 radiation therapy in patients with newly diagnosed glioblastoma multiforme: Final results.  
639 *Neuro-Oncology* **8**, 448-448 (2006).
- 640 22 Peereboom, D. M. *et al.* Phase II trial of erlotinib with temozolomide and radiation in  
641 patients with newly diagnosed glioblastoma multiforme. *Journal of neuro-oncology* **98**, 93-99  
642 (2010).
- 643 23 Vogelbaum, M., Peereboom, D., Stevens, G., Barnett, G. & Brewer, C. Phase II study of  
644 erlotinib single agent therapy in recurrent glioblastoma multiforme. *Ejc*  
645 *Supplementaryments* **3**, 135-135 (2005).
- 646 24 Vogelbaum, M. A., Peereboom, D., Stevens, G., Barnett, G. & Brewer, C. Phase II trial of the  
647 EGFR tyrosine kinase inhibitor erlotinib for single agent therapy of recurrent Glioblastoma  
648 Multiforme: Interim results. *Journal of Clinical Oncology* **22**, 121s-121s (2004).
- 649 25 Vogelbaum, M. A., Peereboom, D., Stevens, G. H., Barnett, G. H. & Brewer, C. Phase II study  
650 of single agent therapy with the EGFR tyrosine kinase inhibitor erlotinib in recurrent  
651 Glioblastoma Multiforme. *Annals of Oncology* **15**, 206-207 (2004).
- 652 26 Vogelbaum, M. A., Peereboom, D., Stevens, G. H. J., Barnett, G. H. & Brewer, C. Response  
653 rate to single agent therapy with the EGFR tyrosine kinase inhibitor erlotinib in recurrent  
654 glioblastoma multiforme: Results of a phase II study. *Neuro-Oncology* **6**, 384-384 (2004).
- 655 27 Lassman, A. B., Abrey, L. E. & Gilbert, M. R. Response of glioblastomas to EGFR kinase  
656 inhibitors. *The New England journal of medicine* **354**, 525-526; author reply 525-526 (2006).
- 657 28 Norden, A. D. *et al.* Phase II trials of erlotinib or gefitinib in patients with recurrent  
658 meningioma. *J Neurooncol* **96**, 211-217, doi:10.1007/s11060-009-9948-7 (2010).
- 659 29 Raizer, J. J. *et al.* A phase II trial of erlotinib in patients with recurrent malignant gliomas and  
660 nonprogressive glioblastoma multiforme postradiation therapy. *Neuro Oncol* **12**, 95-103,  
661 doi:10.1093/neuonc/nop015 (2010).
- 662 30 Raizer, J. J. *et al.* A phase I trial of erlotinib in patients with nonprogressive glioblastoma  
663 multiforme postradiation therapy, and recurrent malignant gliomas and meningiomas.  
664 *Neuro Oncol* **12**, 87-94, doi:10.1093/neuonc/nop017 (2010).
- 665 31 Takano, S. *et al.* Concentration of vascular endothelial growth factor in the serum and tumor  
666 tissue of brain tumor patients. *Cancer research* **56**, 2185-2190 (1996).
- 667 32 Plate, K. H. & Risau, W. Angiogenesis in malignant gliomas. *Glia* **15**, 339-347 (1995).
- 668 33 Zhou, Y.-H., Tan, F., Hess, K. R. & Yung, W. K. A. The expression of PAX6, PTEN, vascular  
669 endothelial growth factor, and epidermal growth factor receptor in gliomas: relationship to  
670 tumor grade and survival. *Clinical cancer research : an official journal of the American*  
671 *Association for Cancer Research* **9**, 3369-3375 (2003).
- 672 34 Chaudhry, I. H., O'Donovan, D. G., Brenchley, P. E., Reid, H. & Roberts, I. S. Vascular  
673 endothelial growth factor expression correlates with tumour grade and vascularity in  
674 gliomas. *Histopathology* **39**, 409-415 (2001).
- 675 35 Lai, A. *et al.* Phase II study of bevacizumab plus temozolomide during and after radiation  
676 therapy for patients with newly diagnosed glioblastoma multiforme. *Journal of clinical*  
677 *oncology : official journal of the American Society of Clinical Oncology* **29**, 142-148 (2011).
- 678 36 Gilbert, M. R. *et al.* A randomized trial of bevacizumab for newly diagnosed glioblastoma.  
679 *The New England journal of medicine* **370**, 699-708 (2014).
- 680 37 Hamerlik, P. *et al.* Autocrine VEGF-VEGFR2-Neuropilin-1 signaling promotes glioma stem-like  
681 cell viability and tumor growth. *J Exp Med* **209**, 507-520, doi:10.1084/jem.20111424 (2012).
- 682 38 Yu, Y. *et al.* Knockdown of vascular endothelial cell growth factor expression sensitizes U251  
683 glioma cells to liposomal paclitaxel and radiation treatment in vitro. *Exp Ther Med* **3**, 181-  
684 186, doi:10.3892/etm.2011.379 (2012).

- 685 39 Fael Al-Mayhany, T. M. *et al.* An efficient method for derivation and propagation of  
686 glioblastoma cell lines that conserves the molecular profile of their original tumours. *Journal*  
687 *of neuroscience methods* **176**, 192-199 (2009).
- 688 40 Subiel, A., Ashmore, R. & Schettino, G. Standards and Methodologies for Characterizing  
689 Radiobiological Impact of High-Z Nanoparticles. *Theranostics* **6**, 1651-1671,  
690 doi:10.7150/thno.15019 (2016).
- 691 41 Hirai, H. *et al.* MK-2206, an allosteric Akt inhibitor, enhances antitumor efficacy by standard  
692 chemotherapeutic agents or molecular targeted drugs in vitro and in vivo. *Mol Cancer Ther* **9**,  
693 1956-1967, doi:10.1158/1535-7163.MCT-09-1012 (2010).
- 694 42 Hickson, I. *et al.* Identification and characterization of a novel and specific inhibitor of the  
695 ataxia-telangiectasia mutated kinase ATM. *Cancer Res* **64**, 9152-9159, doi:10.1158/0008-  
696 5472.CAN-04-2727 (2004).
- 697 43 Subramanian, A. *et al.* Gene set enrichment analysis: a knowledge-based approach for  
698 interpreting genome-wide expression profiles. *Proc Natl Acad Sci U S A* **102**, 15545-15550,  
699 doi:10.1073/pnas.0506580102 (2005).
- 700 44 Banath, J. P., Macphail, S. H. & Olive, P. L. Radiation sensitivity, H2AX phosphorylation, and  
701 kinetics of repair of DNA strand breaks in irradiated cervical cancer cell lines. *Cancer Res* **64**,  
702 7144-7149, doi:10.1158/0008-5472.CAN-04-1433 (2004).
- 703 45 Weterings, E. & Chen, D. J. The endless tale of non-homologous end-joining. *Cell research* **18**,  
704 114-124 (2008).
- 705 46 Vitale, I., Galluzzi, L., Castedo, M. & Kroemer, G. Mitotic catastrophe: a mechanism for  
706 avoiding genomic instability. *Nat Rev Mol Cell Biol* **12**, 385-392, doi:10.1038/nrm3115 (2011).
- 707 47 Mannino, M., Gomez-Roman, N., Hochegger, H. & Chalmers, A. J. Differential sensitivity of  
708 Glioma stem cells to Aurora kinase A inhibitors: implications for stem cell mitosis and  
709 centrosome dynamics. *Stem cell research* **13**, 135-143 (2014).
- 710 48 Neal, J. A. *et al.* Inhibition of homologous recombination by DNA-dependent protein kinase  
711 requires kinase activity, is titratable, and is modulated by autophosphorylation. *Molecular*  
712 *and cellular biology* **31**, 1719-1733 (2011).
- 713 49 Neal, J. A. *et al.* Unraveling the complexities of DNA-dependent protein kinase  
714 autophosphorylation. *Molecular and cellular biology* **34**, 2162-2175 (2014).
- 715 50 Kakarougkas, A. & Jeggo, P. A. DNA DSB repair pathway choice: an orchestrated handover  
716 mechanism. *Br J Radiol* **87**, 20130685, doi:10.1259/bjr.20130685 (2014).
- 717 51 Toulany, M. *et al.* Targeting of AKT1 enhances radiation toxicity of human tumor cells by  
718 inhibiting DNA-PKcs-dependent DNA double-strand break repair. *Molecular cancer*  
719 *therapeutics* **7**, 1772-1781 (2008).
- 720 52 Toulany, M. *et al.* Akt promotes post-irradiation survival of human tumor cells through  
721 initiation, progression, and termination of DNA-PKcs-dependent DNA double-strand break  
722 repair. *Molecular cancer research : MCR* **10**, 945-957 (2012).
- 723 53 Vartak, S. V. & Raghavan, S. C. Inhibition of nonhomologous end joining to increase the  
724 specificity of CRISPR/Cas9 genome editing. *FEBS J* **282**, 4289-4294, doi:10.1111/febs.13416  
725 (2015).
- 726 54 Lombardi, G. *et al.* Updated results of REGOMA: A randomized, multicenter, controlled  
727 open-label phase II clinical trial evaluating regorafenib in relapsed glioblastoma (GBM)  
728 patients (PTS). *Journal of Clinical Oncology* **36**, 2047-2047,  
729 doi:10.1200/JCO.2018.36.15\_Supplementary.2047 (2018).
- 730 55 Friedmann, B. J. *et al.* Interaction of the epidermal growth factor receptor and the DNA-  
731 dependent protein kinase pathway following gefitinib treatment. *Molecular cancer*  
732 *therapeutics* **5**, 209-218 (2006).
- 733 56 Dittmann, K., Mayer, C., Kehlbach, R. & Rodemann, H. P. Radiation-induced caveolin-1  
734 associated EGFR internalization is linked with nuclear EGFR transport and activation of DNA-  
735 PK. *Molecular cancer* **7**, 69 (2008).

- 736 57 Cheng, Y. *et al.* MK-2206, a novel allosteric inhibitor of Akt, synergizes with gefitinib against  
737 malignant glioma via modulating both autophagy and apoptosis. *Mol Cancer Ther* **11**, 154-  
738 164, doi:10.1158/1535-7163.MCT-11-0606 (2012).
- 739 58 Narayan, R. S. *et al.* The allosteric AKT inhibitor MK2206 shows a synergistic interaction with  
740 chemotherapy and radiotherapy in glioblastoma spheroid cultures. *BMC Cancer* **17**, 204,  
741 doi:10.1186/s12885-017-3193-9 (2017).
- 742 59 Dittmann, K. *et al.* Nuclear EGFR shuttling induced by ionizing radiation is regulated by  
743 phosphorylation at residue Thr654. *FEBS letters* **584**, 3878-3884 (2010).

744

## 745 **Figure legends**

746 **Figure 1.** Radiosensitisation of GSC is determined by growth conditions. **A-B**,  
747 Clonogenic efficiency (A) and survival (B) of G7, E2 and R10 GSC grown in 2D and  
748 3D conditions with or without VEGF (3 ng/ml) and irradiated with single doses of X-  
749 rays (0-6 Gy;  $n=3$ ). VEGF deprivation significantly increased radiosensitivity of G7,  
750 E2 and R10 GSC under 3D conditions (two way ANOVA;  $p=0.0009$ ,  $p=0.0056$ , and  
751  $p < 0.0001$ , respectively). No significant effect of VEGF was observed in 2D  
752 conditions. **C**, Western blot analysis of G7 GSC grown in 2D or 3D conditions and  
753 treated with IR (5 Gy) and/or erlotinib (1  $\mu$ M) at the indicated time points. Actin  
754 served as loading control. **D**, Clonogenic survival curves as in (B). Cells were  
755 treated with erlotinib (1  $\mu$ M) for 2 h and then irradiated at different radiation doses (0-  
756 6 Gy). All cell lines grown in 2D conditions were significantly radiosensitised by  
757 erlotinib (2-way ANOVA analysis: G7  $p < 0.0001$ , E2  $p < 0.001$ , R10  $p < 0.01$ ). No  
758 radiosensitisation was conferred upon 3D GSC by erlotinib.

759 **Figure 2.** Akt regulates EGFR and VEGF radiosensitivity in 2D and 3D GSC,  
760 respectively. **A**, G7 and E2 cells grown in 2D or 3D conditions were growth factor-  
761 starved for 48 hours followed by addition of EGF (10 ng/ml) or VEGF (3 ng/ml). Cell  
762 extracts were prepared at the indicated time points and analysed for total and  
763 phospho-EGFR (Y1173) and total and phospho-Akt (S473). S = serum starved; GF =

764 +EGF and +VEGF for 6 hours. Actin served as loading control. **B**, Protein extracts of  
765 G7 (upper blots) and E2 GSCs (lower blots) grown in 2D and 3D conditions in the  
766 presence of VEGF and treated for 2 hrs with erlotinib at a range of concentrations  
767 (0.5 to 5  $\mu$ M) followed by radiation treatment (5 Gy) or mock-irradiation. Lysates  
768 were prepared 1 hour after irradiation and analysed for total and phosphorylated  
769 EGFR and Akt. **C**, E2 GSCs grown in 2D and 3D conditions in the presence of VEGF  
770 were treated with vehicle (DMSO) or erlotinib (1  $\mu$ M) for 2 hrs and ionising radiation  
771 (5 Gy) and protein extracts obtained at different time points after irradiation and  
772 analysed as in A. **D**, G7 and E2 GSC grown in 2D and 3D conditions in the presence  
773 of VEGF were treated with MK-2206 (1  $\mu$ M) for 2 hours mock-irradiated or treated  
774 with ionising radiation (5 Gy). Protein extracts were prepared at different time points.  
775 Samples were analysed for total and activated Akt (pAkt at S473) and  $\gamma$ H2AX by  
776 Western blot. Tubulin served as loading control.

777 **Figure 3.** Radiosensitisation of GSC by Akt inhibition. **A**, Clonogenic survival of G7  
778 and E2 GSC grown in 2D conditions and irradiated with single doses of X-rays (0-6  
779 Gy;  $n=3$ ) 1 h after treatment with DMSO, MK-2206 (1  $\mu$ M) and/or erlotinib (1 $\mu$ M).  
780 MK-2206 treatment significantly increased radiosensitivity of G7 and E2 GSC in 2D  
781 (two-way ANOVA; G7 2D vs G7 2D + MK-2206 or G7 2D + erlotinib + MK2206  
782  $p<0.0001$ ; E2 2D vs E2 + MK-2206 or E2 2D + MK-2206 + erlotinib  $p <0.0001$ , E2  
783 2D vs E2 + erlotinib  $p = 0.0006$ ). **B**, Clonogenic survival of G7 and E2 GSC grown in  
784 3D in conditions as in (A). MK-2206 treatment significantly increased radiosensitivity  
785 of G7 and E2 GSC in 3D conditions (two-way ANOVA; G7 3D vs G7 3D + MK-2206  
786 (+) VEGF or G7 3D + MK2206 (-) VEGF  $p<0.0001$ ; E2 3D vs all other conditions  $p$   
787  $<0.0001$ .) **C**, MK-2206 dose response (0.1  $\mu$ M to 10  $\mu$ M) at 0 and 3 Gy in G7 3D  
788 GSC. Each curve is normalised to respective vehicle plus radiation dose. **D**, Cell

789 lysates from E2 cells transfected with siRNA against Akt1, Akt3 or Scramble were  
790 analysed for expression of total Akt1, Akt3 after 48 h incubation. Tubulin served as  
791 loading control. **E**, Clonogenic assays were performed from E2 cells previously  
792 transfected with Scramble or Akt1-3 siRNAs. Akt siRNA cells exhibited increased  
793 radiosensitivity compared to Scramble siRNA (two-way ANOVA; siRNA Scramble v  
794 all three siRNA Akts  $p < 0.0001$ ).

795 **Figure 4.** VEGF deprivation and Akt inhibition reduce DNA double strand break  
796 repair following irradiation, of 3D GSC. **A**, Representative immunofluorescent images  
797 for  $\gamma$ H2AX foci of G7 GSC grown in 3D conditions before (0 h) or after (24 h) ionising  
798 radiation (5 Gy) in the presence [(+) VEGF] or absence of VEGF [(-) VEGF]. **B-F**,  
799 Quantification of  $\gamma$ H2AX foci per nucleus following radiation treatment (5 Gy, B, D  
800 and E; or 0 Gy, C and F) in the presence or absence of VEGF (B and C); or DMSO  
801 or MK-2206 (D-F). Median  $\pm$  SD from 3 independent experiments.  $P$  values  
802 calculated by  $t$  test (\*  $p < 0.01$ ; \*\*  $p < 0.001$ ). **G**, Representative images of 3D cells  
803 before and 24 h after irradiation, immunostained for the mitotic marker phospho-S10  
804 histone H3 (green) to visualise mitotic cells. DAPI was used to stain for DNA (blue).  
805 Red arrows indicate cells undergoing mitotic catastrophe. **H**, Percentages of cells  
806 displaying micronuclei, mitosis or mitotic catastrophe. An average of 350  
807 cells/condition/experiment were identified randomly and scored. Mean  $\pm$  SEM of 3  
808 independent experiments.  $P$  values calculated by  $t$  test.

809 **Figure 5.** Functional DNA-PKcs activity correlates with VEGF treatment and Akt  
810 activity in the 3D model. **A and C**, Representative immunofluorescent images of E2  
811 GSC grown in 3D conditions and stained for pDNA-PKcs foci (red) at different time  
812 points following ionising radiation (5 Gy) in the presence or absence of VEGF (A); or

813 DMSO or MK-2206 (C). Cells in C were also immunostained for  $\gamma$ H2AX foci (green).  
814 **B**, Quantification of pDNA-PKcs foci per nucleus following radiation treatment as in **A**.  
815 Graphs represent medians from 3 independent experiments. *P* values calculated by  
816 *t* test (\*  $p < 0.01$ ; \*\*  $p < 0.001$ ; \*\*\*  $P < 0.0001$ ). **D**, Clonogenic assays were performed  
817 with E2 cells previously transfected with either scrambled or DNA-PKcs siRNA for 48  
818 hrs. Transfected cells were treated with MK-2206 (1  $\mu$ M) 16 h after clonogenic  
819 seeding, incubated for 2 hrs and irradiated at different doses (0-5 Gy). Cell lysates  
820 from E2 cells transfected with siRNA against DNA-PKcs or Scramble were analysed  
821 for expression of total DNA-PKcs after 48 hrs incubation. Tubulin served as loading  
822 control. **E**, Representative immunofluorescent images of G7 GSC grown in 3D  
823 conditions for Rad51 foci at 3 hrs following ionising radiation (5 Gy) in the presence  
824 or absence of VEGF. **F**, Quantification of Rad51 foci per nucleus following radiation  
825 treatment. Graph represents mean of medians from 3 independent experiments. *p*  
826 values calculated by *t* test.

827 **Figure 6.** Akt inhibition extends survival of irradiated mice bearing orthotopic glioma  
828 xenografts. **A**, Representative immunofluorescent images of paraffin-embedded  
829 brains bearing E2 orthotopic tumour cells in mice for pDNA-PKcs S2056 (green).  
830 EGFR (red) was used as tumour marker. Mice implanted with E2 cells for 5 months  
831 were treated with radiation (10 Gy) and sacrificed at the indicated time points. **B**,  
832 Diagram of U87MGLuc2 orthotopic efficacy study, depicting treatment schedules (15  
833 mice/cohort). **C**, Graph depicting mouse body weight monitored from cell  
834 implantation until end of treatment. Mice bearing orthotopic xenografts (U87-MGLuc,  
835 13 days after implantation) were randomized into 4 cohorts and treated with the  
836 protocols shown in **B**. **D**, Kaplan-Meier survival curves were generated and analysed  
837 for log-rank. **E**, Box plot graph of median survival of each treatment group, \*  $p < 0.05$ ,

838 \*\*  $p < 0.001$ , \*\*\*  $p < 0.0001$ , by one-way ANOVA original FDR method, multiple  
839 comparison test.

840 **Figure 7.** Erlotinib radioprotects VEGF-deprived 3D GSC by blocking EGFR/DNA-  
841 PKcs nuclear co-localisation. **A**, Clonogenic survival of E2 and G7 GSC grown in 3D  
842 conditions and irradiated with single doses of X-rays (0-6 Gy;  $n=3$ ) 2 hours after  
843 treatment in the presence (+)VEGF or absence (-)VEGF of VEGF and erlotinib (1 $\mu$ M)  
844 or vehicle (DMSO). Mean $\pm$ SD of 3 independent experiments is shown; curves are  
845 fitted to a linear quadratic model. Erlotinib significantly radioprotected VEGF-  
846 deprived cells (two-way ANOVA; G7 3D (-) VEGF vehicle vs G7 3D (-) VEGF plus  
847 erlotinib  $p<0.0001$ , E2,  $p=0.01$ ). No significant effect of erlotinib was observed in the  
848 presence of VEGF. **B** and **C**, Quantification of pDNA-PKcs (B) and Rad51 foci (C)  
849 per nucleus following radiation treatment. Graph represents mean of medians from  
850 3 independent experiments.  $p$  values calculated by  $t$  test (\*  $p < 0.01$ ; \*\*  $p < 0.001$ ).**D**,  
851 Representative immunofluorescent images for EGFR (EGFR) and DNA-PKcs (DNA-  
852 PKcs) of G7 3D cells following ionising radiation treatment and fixed with  
853 paraformaldehyde at the indicated time points (0, 0.5 and 24 hrs). Cells were treated  
854 with erlotinib in the absence or presence of VEGF. **E**, Representative  
855 immunofluorescent images for the co-localisation of DNA-PKcs and EGFR using Zen  
856 Black software by selecting nuclei as regions of interest (red circles) and using the  
857 Cut Mask tool following selection and generation of a new image which sets every  
858 pixel outside the colocalised pixels to zero and exposing only the pixels where tDNA-  
859 PKcs / tEGFR signals are expressed in the same pixel. **F**, Quantification of DNA-  
860 PKcs and EGFR colocalisation per nucleus in G7 3D GSC. Approximately 40 nuclei  
861 were quantified for each condition. Box and whisker plots represent median number  
862 of signal per nucleus,  $p$  values calculated by Mann Whitney  $U$  test (\* $p<0.05$ ;

863 \*\*p<0.005). **G**, Graphic representation of glioblastoma responses to EGF and VEGF  
864 signalling in 2D and 3D conditions, respectively, with Akt acting as the main switch  
865 between NHEJ and HR resulting in radiation sensitization (aberrant NHEJ) or  
866 protection (HR activation).

867

868

869

870

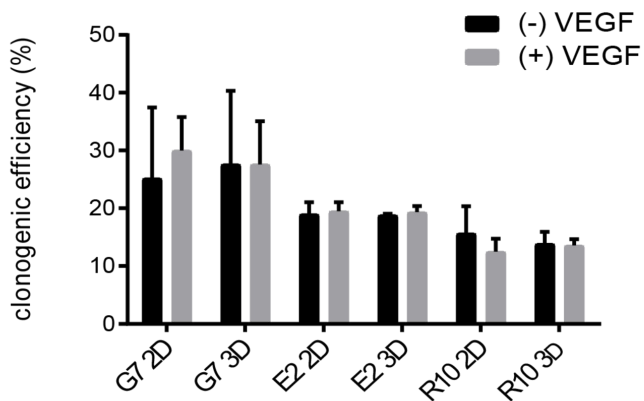
871

872

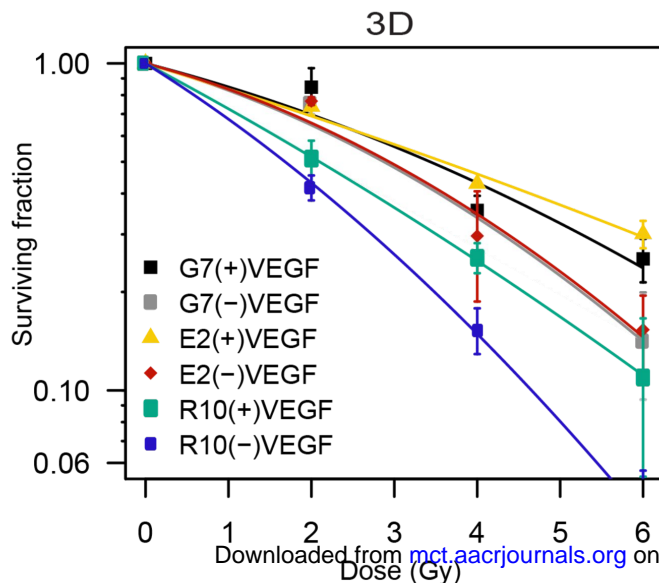
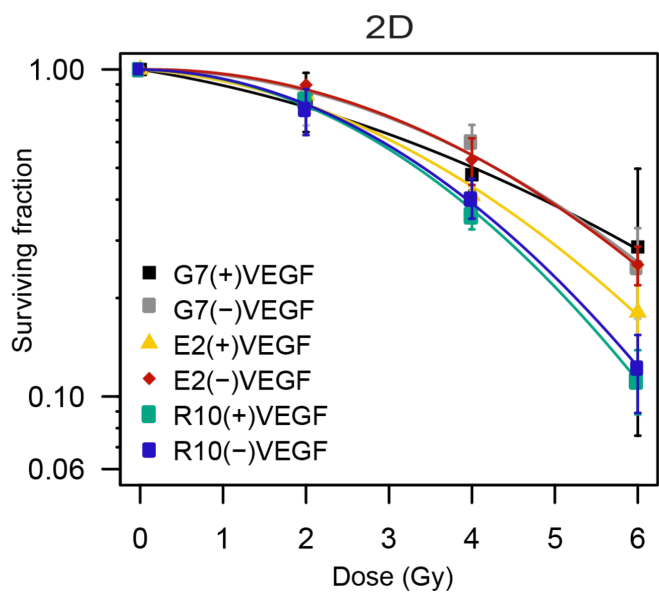
873

Figure 1

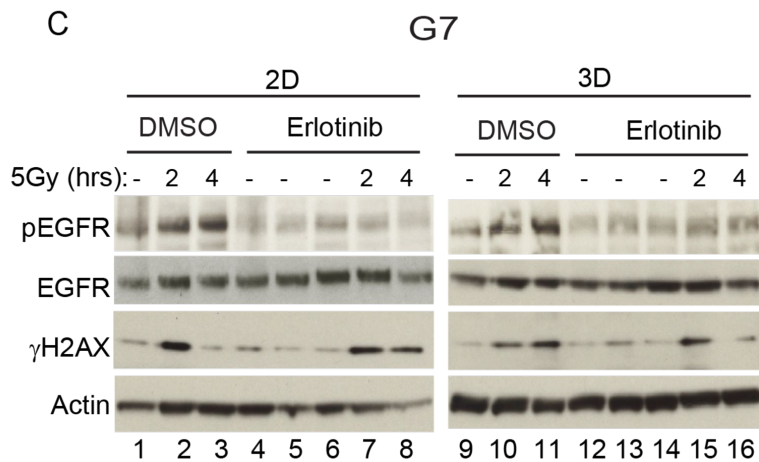
A



B



C



D

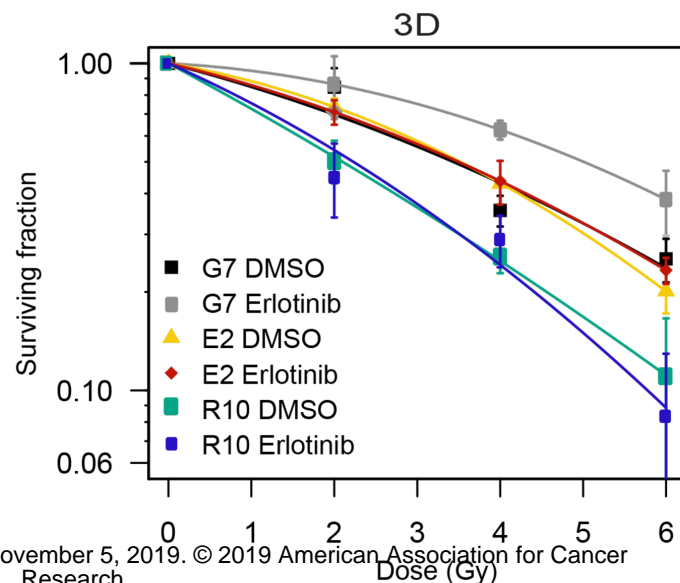
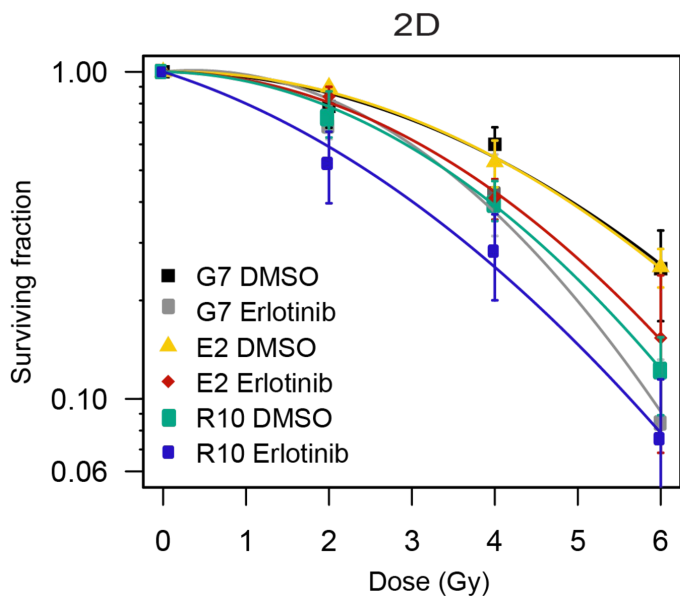
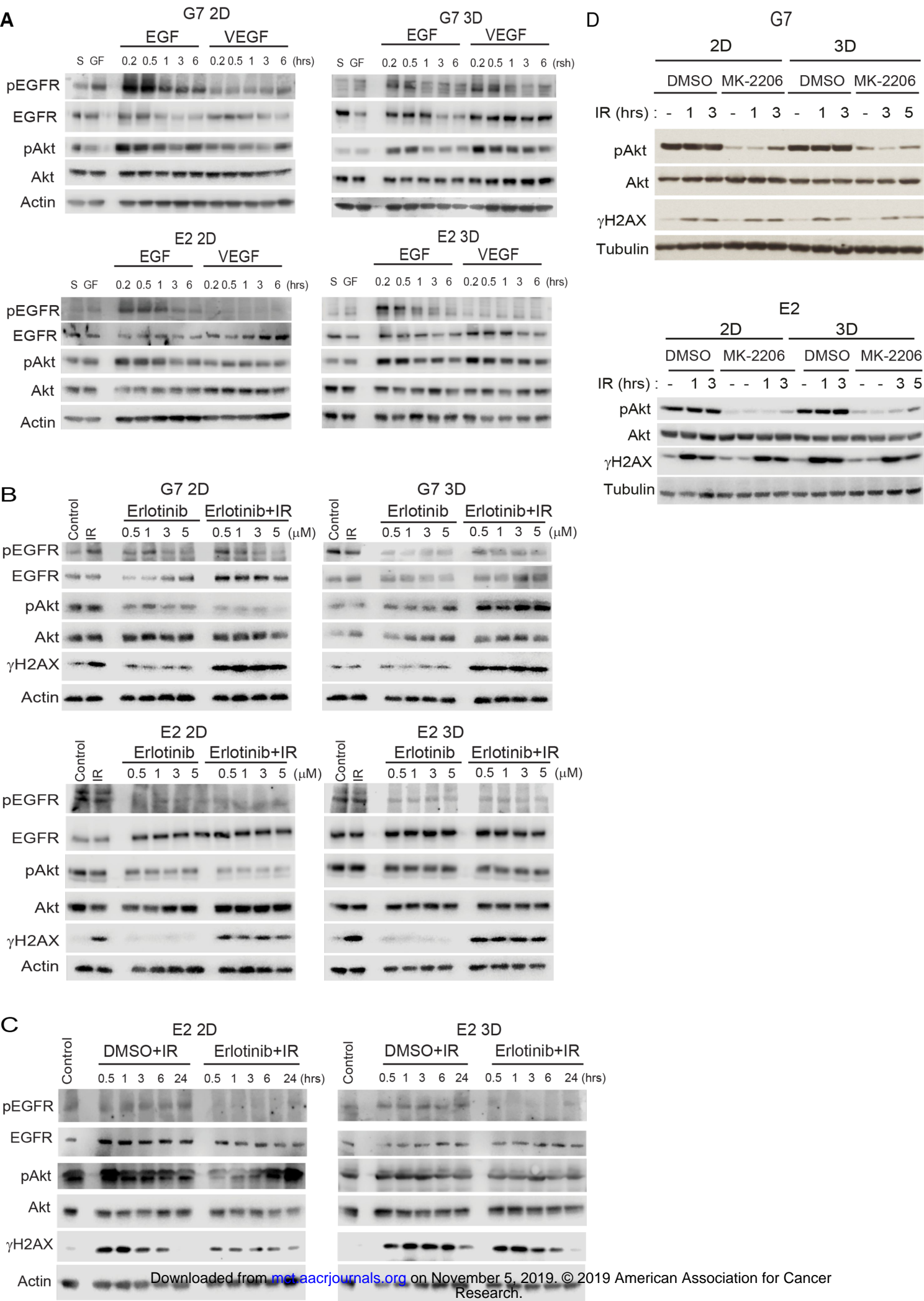
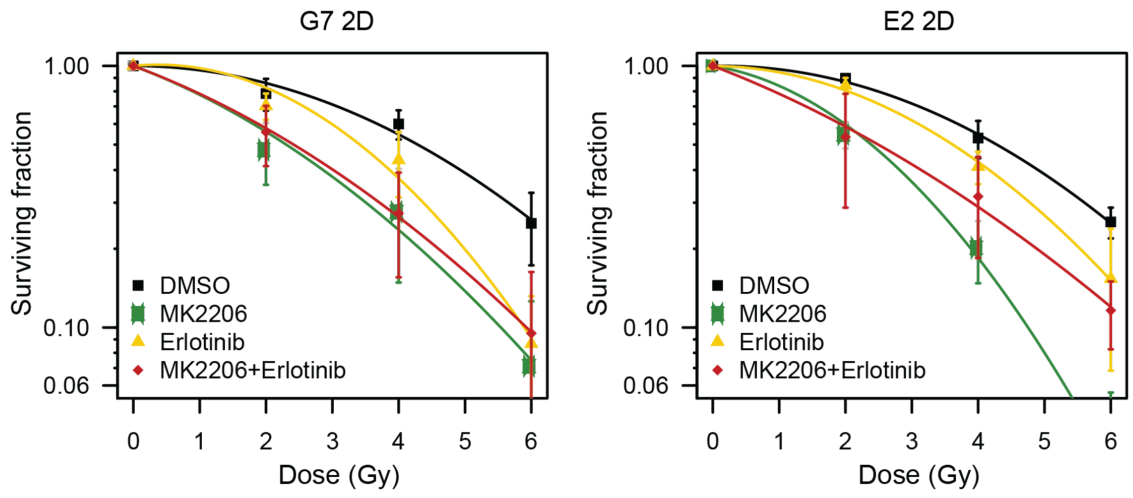


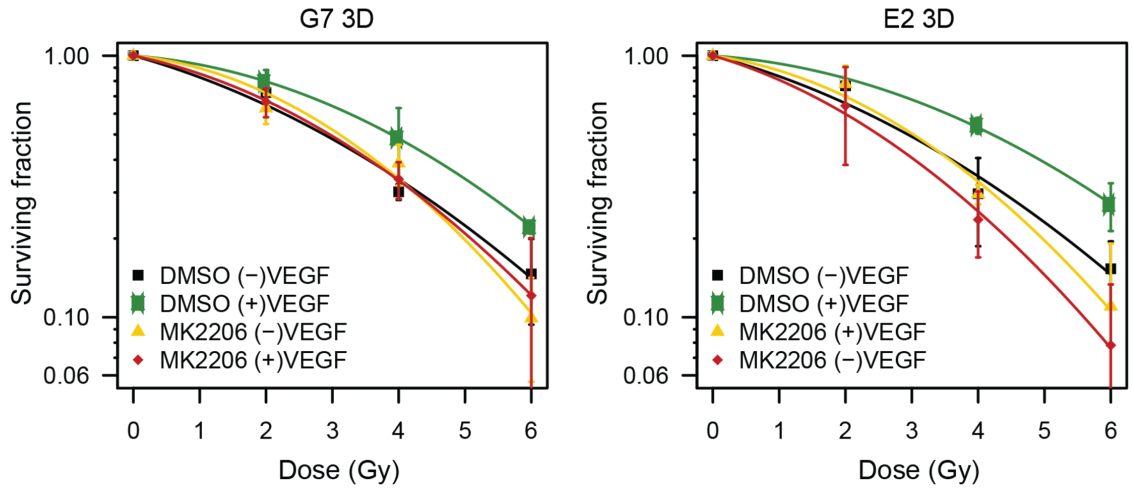
Figure 2



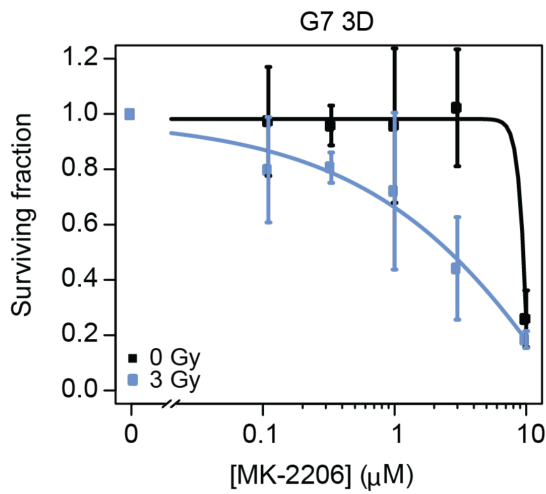
A



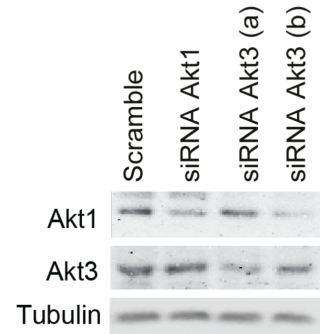
B



C



D



E

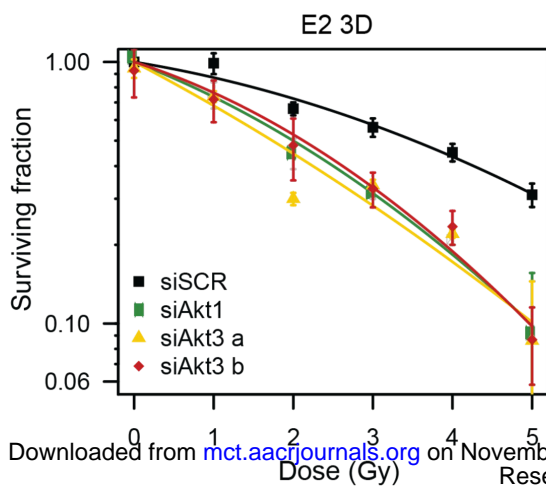


Figure 4

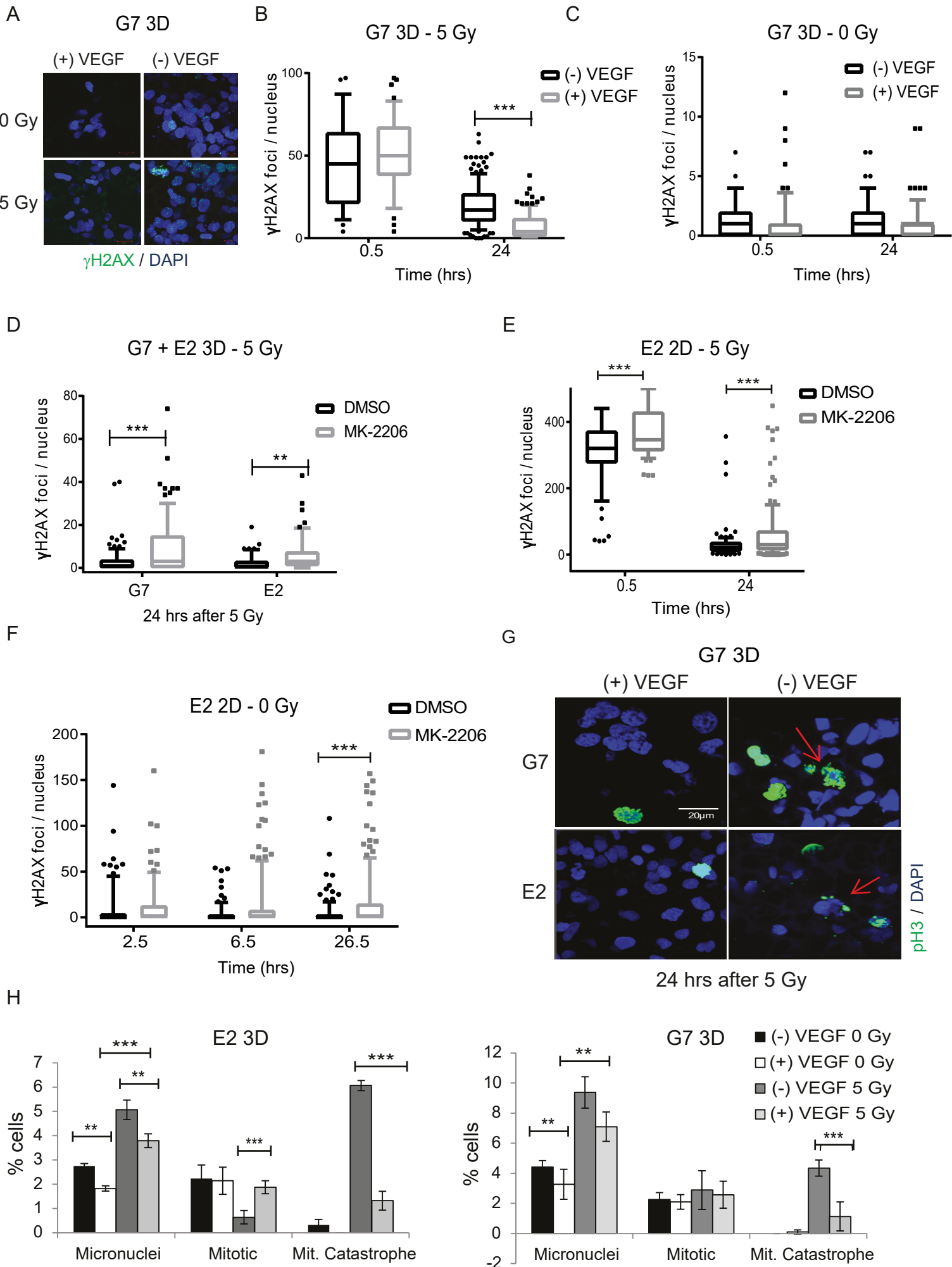
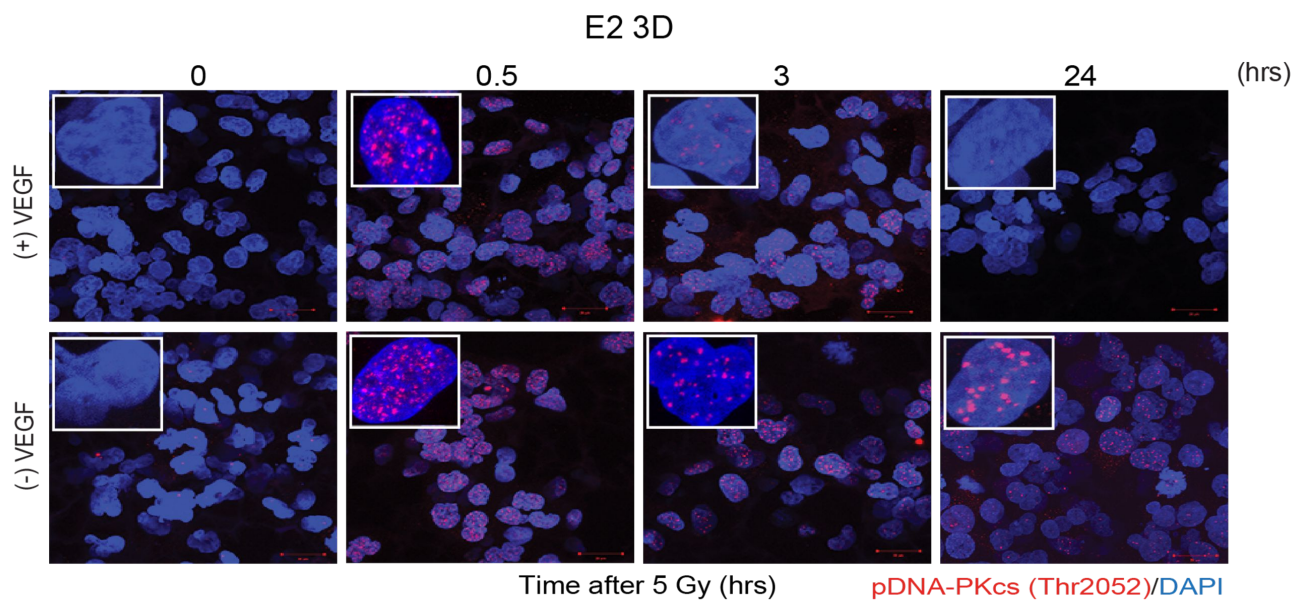
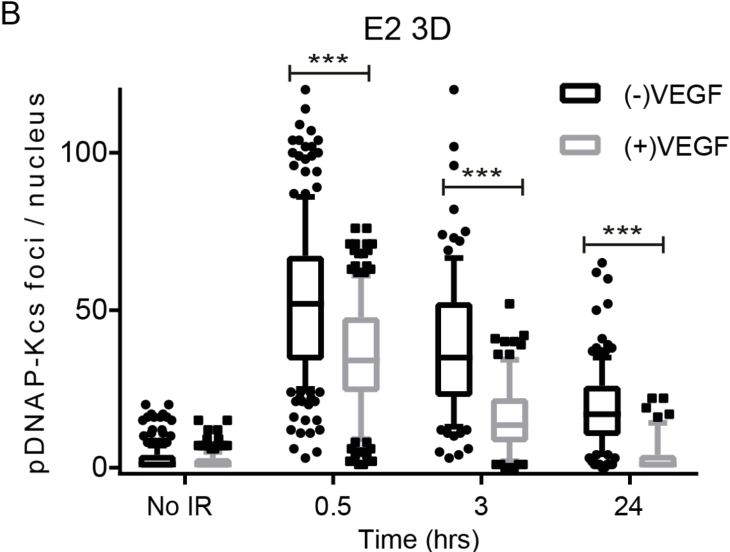


Figure 5

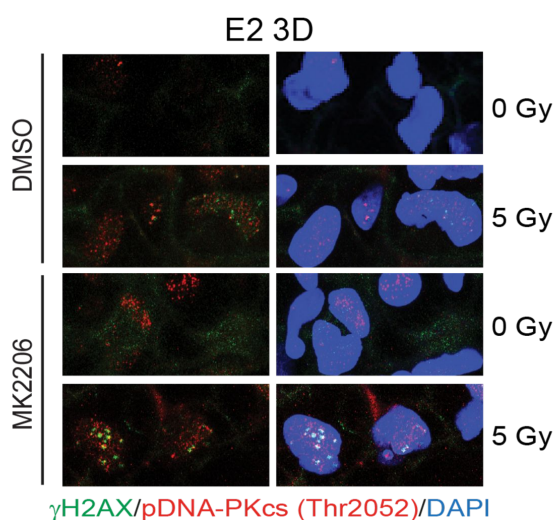
A



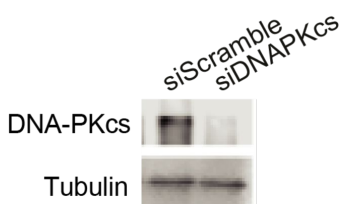
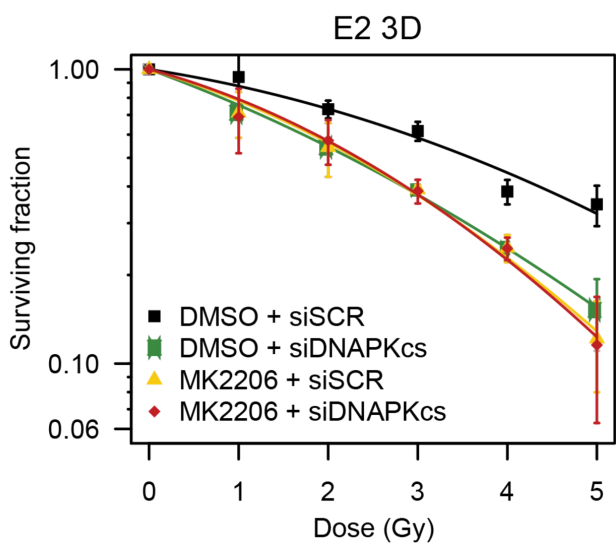
B



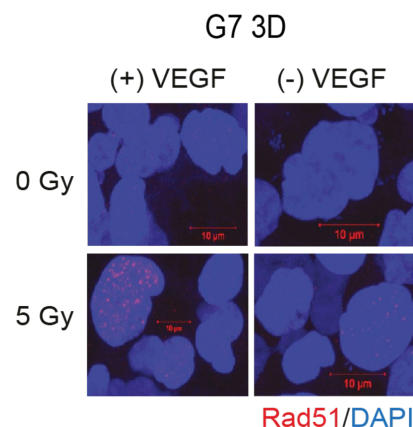
C



D



E



F

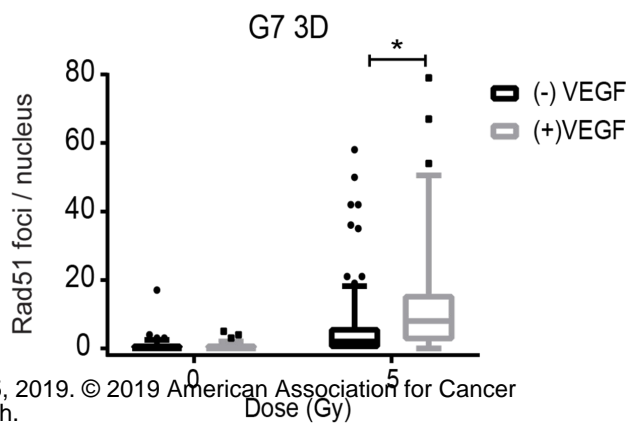
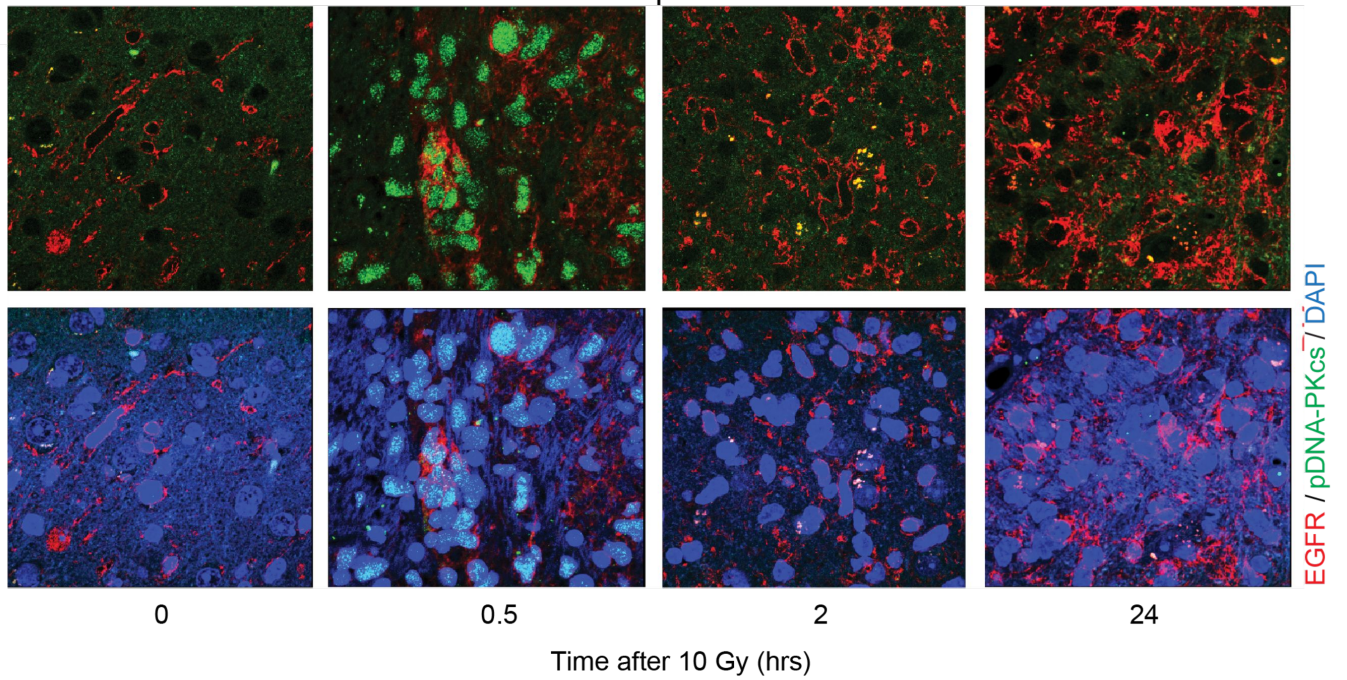


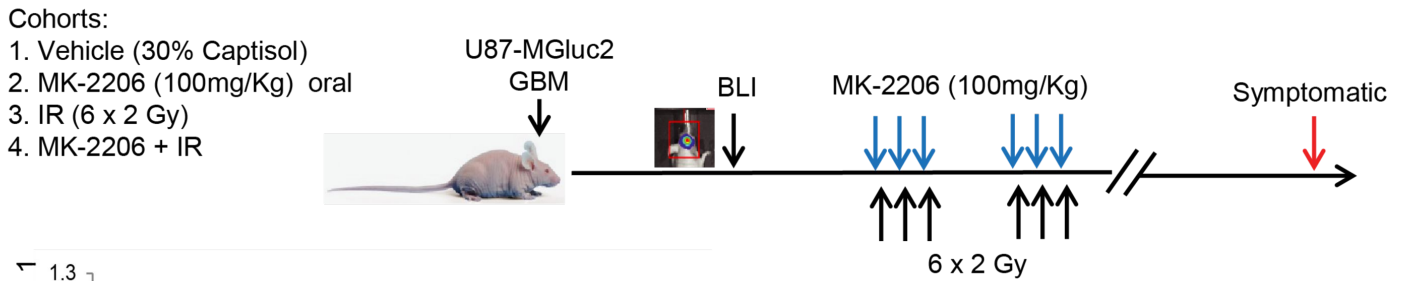
**Figure 6**

**A**

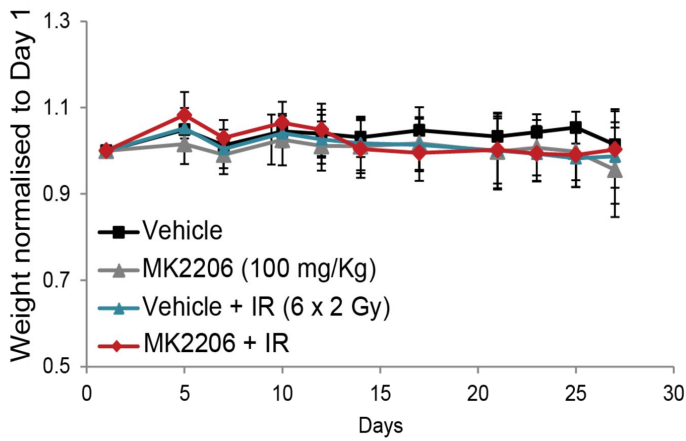
**E2 Orthotopic tumours**



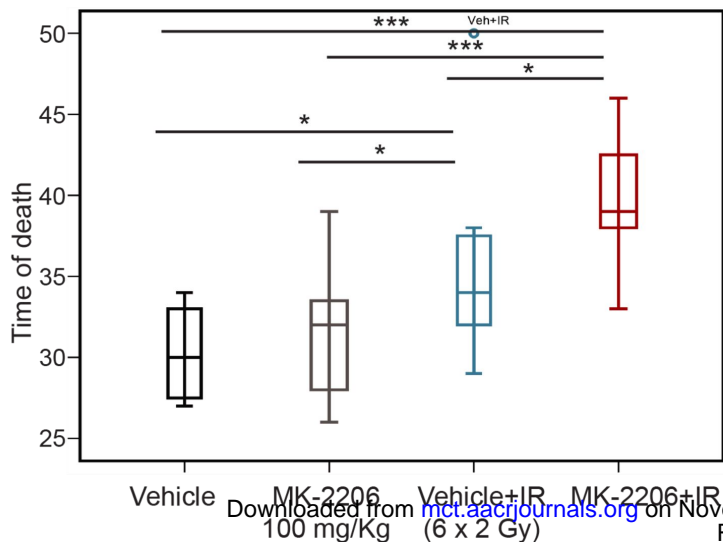
**B**



**C**



**E**



**D**

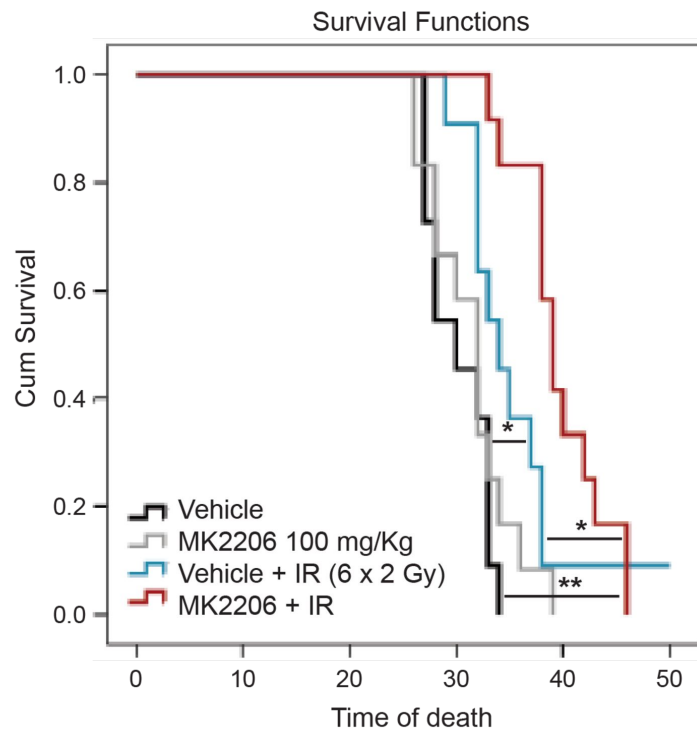
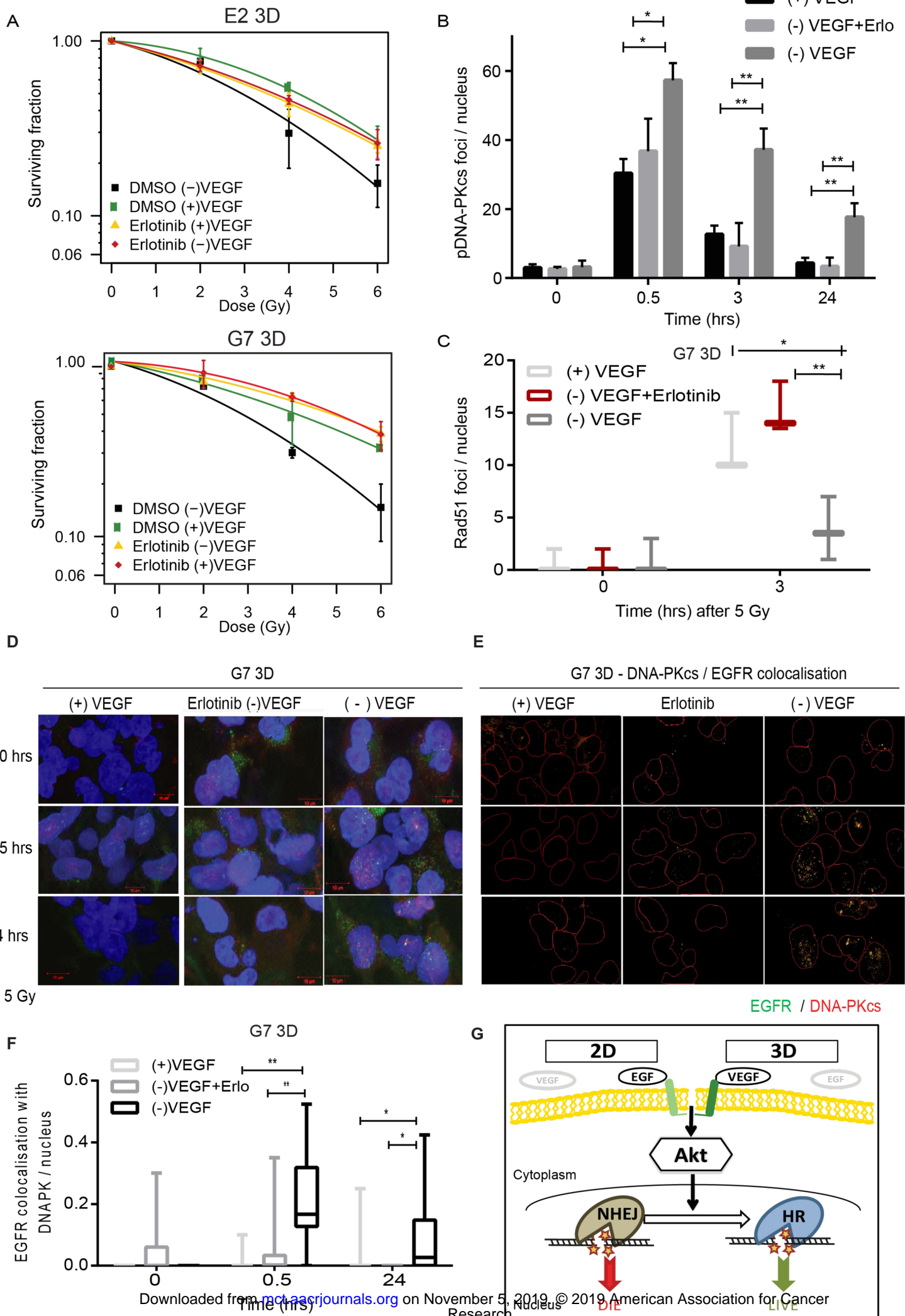


Figure 7



# Molecular Cancer Therapeutics

## Radiation responses of 2D and 3D glioblastoma cells: a novel, 3D-specific radioprotective role of VEGF/Akt signaling through functional activation of NHEJ

Natividad Gomez-Roman, Ming Y Chong, Sandeep K Chahal, et al.

*Mol Cancer Ther* Published OnlineFirst October 31, 2019.

<b>Updated version</b>	Access the most recent version of this article at: doi: <a href="https://doi.org/10.1158/1535-7163.MCT-18-1320">10.1158/1535-7163.MCT-18-1320</a>
<b>Supplementary Material</b>	Access the most recent supplemental material at: <a href="http://mct.aacrjournals.org/content/suppl/2019/10/31/1535-7163.MCT-18-1320.DC1">http://mct.aacrjournals.org/content/suppl/2019/10/31/1535-7163.MCT-18-1320.DC1</a>
<b>Author Manuscript</b>	Author manuscripts have been peer reviewed and accepted for publication but have not yet been edited.

<b>E-mail alerts</b>	<a href="#">Sign up to receive free email-alerts</a> related to this article or journal.
<b>Reprints and Subscriptions</b>	To order reprints of this article or to subscribe to the journal, contact the AACR Publications Department at <a href="mailto:pubs@aacr.org">pubs@aacr.org</a> .
<b>Permissions</b>	To request permission to re-use all or part of this article, use this link <a href="http://mct.aacrjournals.org/content/early/2019/10/31/1535-7163.MCT-18-1320">http://mct.aacrjournals.org/content/early/2019/10/31/1535-7163.MCT-18-1320</a> . Click on "Request Permissions" which will take you to the Copyright Clearance Center's (CCC) Rightslink site.